

A concept of a para-hydrogen-based cold neutron source for simultaneous high flux and high brightness

Alexander Ioffe^{a,*}, Petr Konik^{a,#}, Konstantin Batkov^b

^aJuelich Centre for Neutron Science JCNS at Heinz Maier-Leibnitz Zentrum (MLZ), Lichtenbergstr. 1, 85748, Garching, Germany

^bMAXIV Laboratory, Lund University, Fotongatan 2, 22484, Lund, Sweden

Abstract

A novel concept of cold neutron source employing chessboard or staircase assemblies of high-aspect ratio rectangular para-hydrogen moderators with well-developed and practically fully illuminated surfaces of the individual moderators is proposed.

An analytic approach for calculating the brightness of para-hydrogen moderators is introduced. Because brightness gain originates from a near-the-surface effect resulting from the prevailing single collision process during thermal-to-cold neutron conversion, high-aspect ratio rectangular cold moderators offer a significant increase, up to a factor of 10, in cold neutron brightness compared to a voluminous moderator. The obtained results are in excellent agreement with MCNP calculations.

The chessboard or staircase assemblies of such moderators facilitate the generation of wide neutron beams with simultaneously higher brightness and intensity compared to a para-hydrogen-based cold neutron source made of a single moderator (either flat or voluminous) of the same cross-section. Analytic model calculations indicate that gains of up to approximately 2.5 in both brightness and intensity can be achieved compared to a source made of a single moderator of the same width.

The gain reduction in our study is mostly caused by these two factors: the limited volume of the high-density thermal neutron region surrounding the reactor core or spallation target, which restricts the total length of the moderator assembly, and the finite width of moderator walls. Additional factors affecting gain can be revealed through dedicated Monte Carlo simulations of the moderator-reflector assembly, which can only be conducted for a particular neutron source and are beyond the scope of this general study. Moreover, the relatively large length of moderator assemblies makes their application for short pulse neutron sources very problematic.

The concept of “low-dimensionality” in moderators is explored, demonstrating that achieving a substantial increase in brightness necessitates moderators to be low-dimensional both geometrically, implying a high aspect ratio, and physically, requiring the moderator’s smallest dimension to be smaller than the characteristic scale of moderator medium (about the mean free path for thermal neutrons). This explains why additional compression of the moderator along the longest direction, effectively giving it a tube-like shape, does not result in a significant brightness increase comparable to the flattening of moderator.

Keywords: neutron moderators, para-hydrogen moderators, low-dimensional moderators,

*Corresponding author.

E-mail address: a.ioffe@fz-juelich.de (A. Ioffe)

#Current address: Neutron Spectroscopy Laboratory, HUN-REN Centre for Energy Research, Konkoly-Thege Miklós út, 29–33, 1121, Budapest, Hungary

1. Introduction

Cold neutron sources that provide a high cold neutron flux at neutron scattering instruments are at the core of almost all neutron scattering facilities. They exploit moderators made of a hydrogen-containing material in liquid or solid state at cryogenic temperatures (e.g. hydrogen [1], deuterium [2], methane [3] and others), in which the neutrons emitted from thermal moderators are thermalised down to the temperature of a cold moderator. Recently, low-dimensional para-hydrogen cold moderators were developed at the European Spallation Source (ESS) [4–6]. They employ a remarkable feature of para-hydrogen: the drastic, more than an order of magnitude difference in total neutron scattering cross-sections for cold and thermal neutrons, that leads to the difference in their mean free paths (MFP), about 10 cm and 1 cm, respectively. This allows to squeeze usually large, about $(10 \times 10 \times 10) \text{ cm}^3$, voluminous moderators to the flat shape (so-called pancake geometry [7]), with a height of about 3 cm. This size is enough for thermal neutrons to be effectively slowed down in a single collision to become cold neutrons, which can be extracted along the whole large dimension of the moderator with a low parasitic neutron absorption from para-hydrogen itself [5]. Indeed, the brightness of the neutron beam emitted in this direction is significantly, 2–3 times enhanced in comparison to the brightness of conventional voluminous moderators. Low-dimensional para-hydrogen moderators are now getting more and more attention and are considered for many newly designed high power and compact neutron sources [8–10]. Being used with carefully designed neutron transport systems [11, 12], such moderators can provide 2–3 times gains in flux at samples of neutron instruments requiring well-collimated incident neutron beams.

In Sect. 2 we consider in details the mechanism leading to the increase in brightness of flattened moderators. As thermal to cold neutron conversion in single collision is a unique feature of para-hydrogen (discussed in details in Sect. 4), we develop an analytic model describing the moderators operating exclusively this way. The model predicts significant brightness gains for a moderator with high-aspect ratio viewed surface. The results are confirmed by the corresponding MCNP [13] simulations.

In Sect. 3 we discuss the concept of “low-dimensionality” applied to neutron moderators. We demonstrate that a neutron moderator is low-dimensional and provides significant brightness gain, only if it satisfies both criteria: geometrical low-dimensionality (high aspect ratio) of the viewed surface and physical low-dimensionality, meaning at least one of moderator dimensions is less than the characteristic scale of moderator medium (double MFP for thermal neutrons). Using this concept, we explain why the squeezing of flat moderator to square shape does not provide meaningful brightness gain, as found in [5].

In Sect. 4 we use extensive MCNP calculations to investigate a realistic para-hydrogen moderator and compare it to the previously developed analytic model. We consequently complicate the model by adding realistic illumination by Maxwellian thermal neutron spectrum and actual para-hydrogen scattering cross-section, allowing for multiple collisions process of cold neutron conversion. The qualitative behavior of brightness gains curves for real para-hydrogen is similar to one predicted by the analytic model from Sect. 2 and one can still observe high brightness gains.

In Sect. 5 we briefly overview some properties of the cold neutron spectrum emitted from low-dimensional para-hydrogen moderators.

In Sect. 6 we discuss trade-offs between brightness and intensity of low-dimensional moderators. A significant increase in brightness of the emitted cold neutron beam is achieved at

the cost of a significant reduction in beam intensity. This fact seriously limits the gain in the performance of the intensity-demanding instruments with a low Q -resolution. Moreover, the use of moderators of small size leads to the under-illumination of the entrance of a large neutron guide that in turn results in a very irregular angular structure of neutron beams at samples of high Q -resolution instruments thus worsening their performance [14]. Therefore, it is an imperative to find a possibility to increase the neutron beam intensity while keeping a high brightness of the low dimensional moderators. We propose employing chessboard and staircase assemblies of narrow moderators that provide wide, intense neutron beams while maintaining the high brightness of the narrow moderator.

We also briefly consider the application of such moderators in the case of their inhomogeneous thermal neutron illumination from a nuclear reactor core or a spallation neutron source target. In these cases, the stacked staircase (chessboard) geometry allows for simultaneous gains in brightness and intensity of up to approximately 2.5 for reactor sources and 2 for spallation or compact sources, relative to single flat moderators of the same width. However, these gains will be affected by details of the moderator-reflector assembly and should be estimated through dedicated Monte Carlo simulations, which can only be conducted for a particular neutron source and are beyond the scope of this general study.

2. Analytic model: infinitely thin para-hydrogen moderator

2.1. Brightness calculations for in-plane illumination

To calculate the brightness of a para-hydrogen moderator homogeneously illuminated by thermal neutrons, we start with a simplified model of an isolated, infinitely thin moderator slice cut from the voluminous moderator. This slice is illuminated by thermal neutrons originating from its perimeter (as depicted in Fig. 1).

Initially, we focus on the case where each point of the linear thermal neutron source (represented by red arrows in Fig. 1) emits neutrons isotropically within the xy -plane. We calculate the cold neutron brightness in the z -direction under the assumption that already a single collision with a hydrogen molecule is sufficient to slow down thermal neutrons to cold neutron energies. The validity of this assumption will be verified later in Sect. 4.1, where we analyse the energy losses of neutrons through multiple collisions within the moderator.

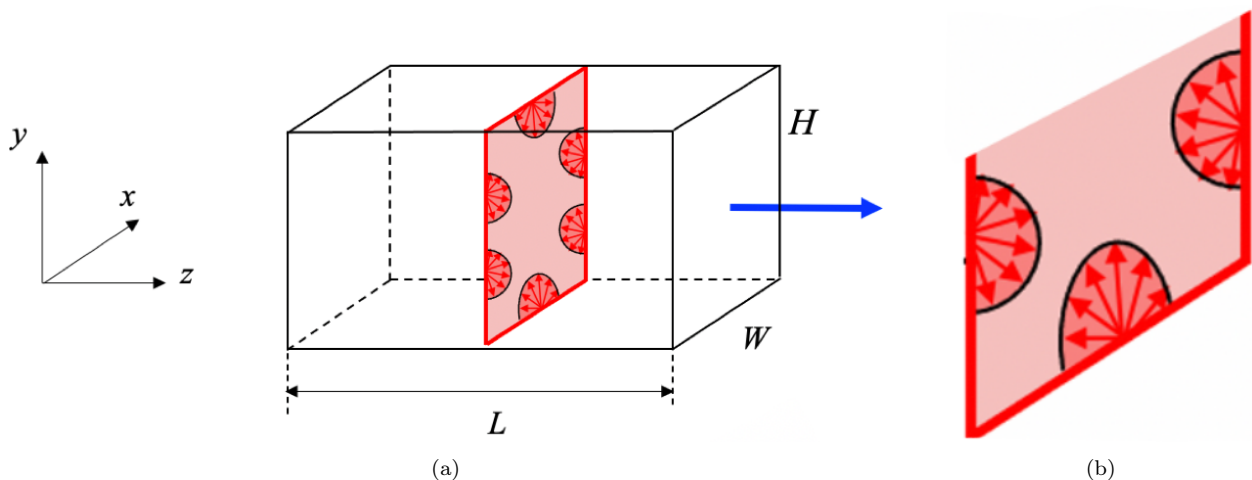


Figure 1: (a) Slice cut from the voluminous cold neutron moderator of a rectangular parallelepiped shape ($W \times H \times L$). Red arrows indicate the directions of thermal neutron illumination, also shown in detail in (b). The blue arrow shows the direction of the outgoing cold neutron beam towards a neutron optical system (e.g., neutron guide).

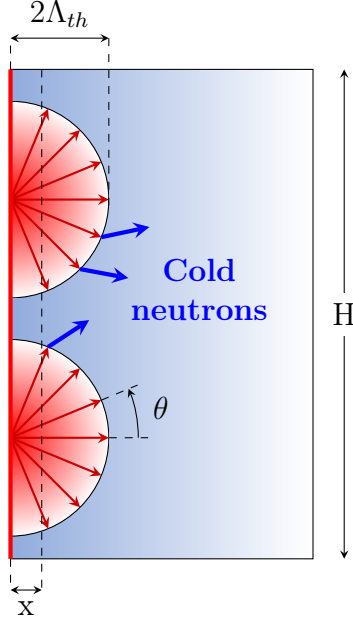


Figure 2: Para-hydrogen moderator illuminated by thermal neutrons emitted from the side wall.

First, we consider a para-hydrogen moderator illuminated by thermal neutrons from one side, so that the side wall can be regarded as an isotropic neutron source and investigate where and how cold neutrons are produced. For this reason we examine the near-the-surface layer of thickness x (Fig. 2). Thermal neutrons are propagating over path s , that length depends on both the layer thickness x and the emission angle θ as $s = x/\cos(\theta)$.

If a source element dh emits neutrons within an angular range $d\theta$, then the beam's intensity can be expressed as follows:

$$dI_{th0} = B_{th0} dh d\theta, \quad (1)$$

where B_{th0} is the brightness of a homogeneous isotropic linear source.

The neutron transmission after the propagation over the path s is equal to $\exp(-s/\Lambda_{th})$, where Λ_{th} is the mean free path of thermal neutrons in para-hydrogen, so that the intensity of the thermal neutron beam is equal to

$$dI_{th}(x, \theta) = dI_{th0} \exp\left(-\frac{x}{\Lambda_{th} \cos \theta}\right), \quad (2)$$

where the initial intensity of the thermal beam is given in Eq. (1).

The intensity $dI_{cold}(x, \theta)$ of the beam comprised of neutrons that have undergone collisions with the hydrogen molecules is defined by reduction in thermal neutron beam intensity:

$$\begin{aligned} dI_{cold}(x, \theta) &= dI_{th0} - dI_{th}(x, \theta) = \\ &= dI_{th0} \left(1 - \exp\left(-\frac{x}{\Lambda_{th} \cos \theta}\right)\right) = \\ &= B_{th0} \left(1 - \exp\left(-\frac{x}{\Lambda_{th} \cos \theta}\right)\right) dh d\theta. \end{aligned} \quad (3)$$

Since we assumed that thermal neutrons are slowed down to cold energies already as the result of a single collision (see Sect. 4.3 and Sect. 4.4 for more details), $dI_{cold}(x, \theta)$ represents the intensity of the cold neutron beam produced within a layer of thickness x

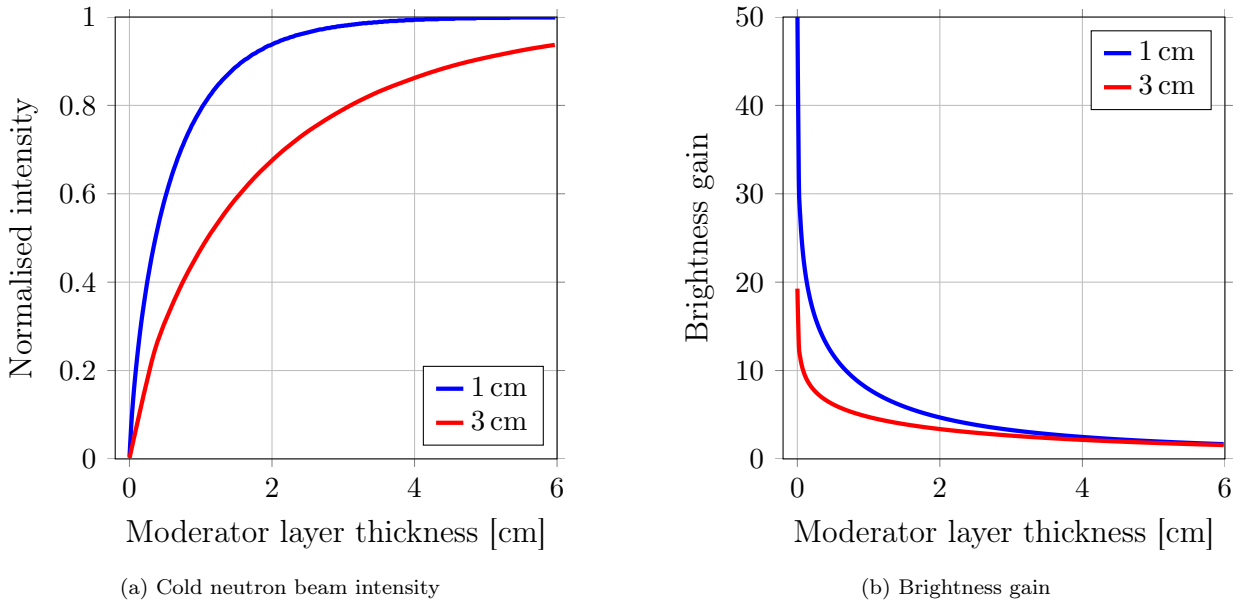


Figure 3: Intensity of the cold neutron beam (a) and gain in brightness (b) as functions of the moderator layer thickness x for thermal neutrons with mean free path $\Lambda_{th} = 1$ cm (blue curves) and $\Lambda_{th} = 3$ cm (red curves). The plots are normalised to the moderator of $x = 10$ cm thickness.

from the thermal neutrons emitted with the initial direction θ by a perimeter element dh . Total intensity I_{cold} of the cold neutron beam produced within such layer is obtained by integrating Eq. (3) over θ and h :

$$I_{cold}(x) = B_{th0} \int_0^H \int_{-\pi/2}^{\pi/2} \left(1 - \exp\left(-\frac{x}{\Lambda_{th} \cos \theta}\right) \right) dh d\theta \quad (4)$$

Here for simplicity we neglect the edge effects at the very top and bottom of the moderator (Fig. 2), where thermal neutrons with some directions θ can't contribute to the production of cold neutrons. However, these effects will be taken into account in further calculations in Sect. 2.2.

The brightness of such cold neutron source is determined by dividing intensity of the cold neutron beam by the size of the source:

$$B_{cold}(x) = \frac{I_{cold}(x)}{4\pi H x}. \quad (5)$$

The dependence $I_{cold}(x)$ is shown in Fig. 3a. One can see that about 95% of thermal neutrons are converted to cold ones within the layer of $x = 2\Lambda_{th}$, so that there is no significant increase in the cold neutron intensity for $x > 2\Lambda_{th}$. The red curve represents the behavior of neutrons with a mean free path of $\Lambda_{th} = 1$ cm, while the blue curve corresponds to neutrons with a mean free path of $\Lambda_{th} = 3$ cm. These mean free path values are associated with a scattering cross-section σ of 23.9 b in para-hydrogen for neutrons with an energy of 60 meV (approximately corresponding to the peak of the ESS water pre-moderator spectrum [6, Figure 10]) and 25 meV, which is the most probable energy of neutron spectra from H₂O or D₂O moderators in steady power reactors at a temperature of 300 K.

As the value of x approaches zero, the numerator in Eq. (5) falls at a slower rate than a linear function in denominator, so that the brightness $B_{cold}(x)$ exhibits a significant increase (Fig. 3b).

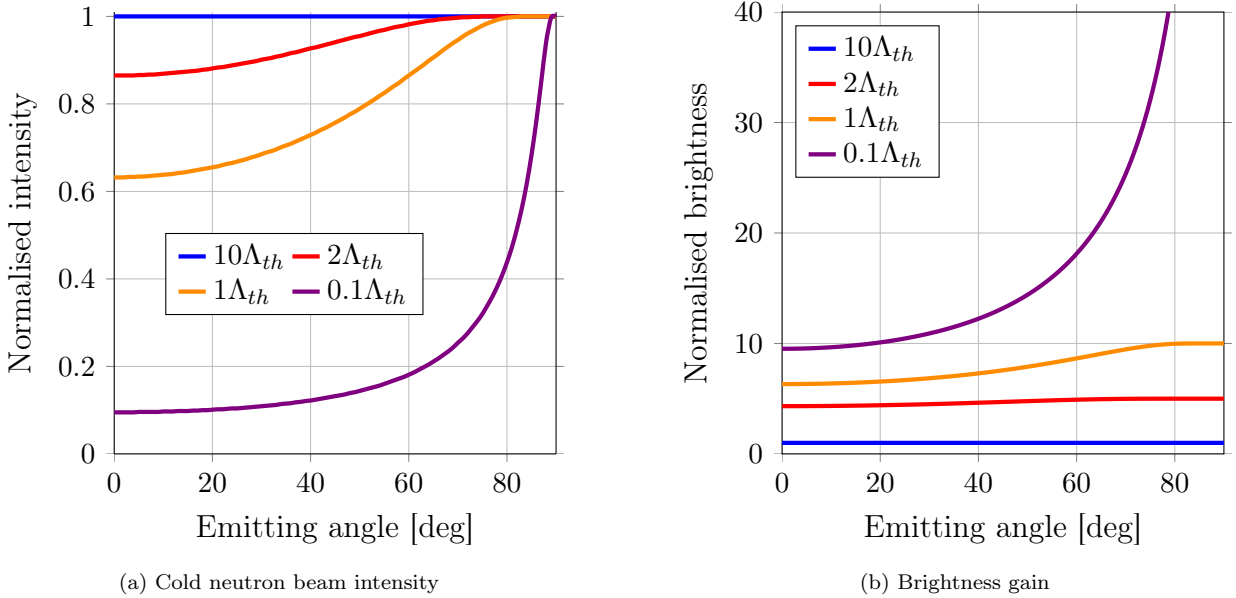


Figure 4: Intensity and brightness of the produced cold beam as functions of the emitting angle θ for different moderator thicknesses.

Let us consider cold moderator which width exactly matches the thickness x of previously considered layer. Then we can conclude that in the case of narrow moderators with a width $x \ll \Lambda_{th}$, only “grazing” thermal neutrons, which propagate almost parallel to the moderator wall with θ close to $\pm\pi/2$, have high probability of colliding with hydrogen atoms and converting to cold neutrons. This phenomenon is demonstrated by the angular dependence of cold neutron intensity (see Eq. (3)) for different thicknesses of the moderator layer (Fig. 4a): the “grazing” neutrons contribute significantly to the total cold neutron beam intensity, leading to a substantial increase in brightness for narrow moderators. This can be observed in Fig. 4b by comparing the curves for $x = 2\Lambda_{th}$, which roughly represents the thickness of the flat cold moderator at ESS [6], and $x = 0.1\Lambda_{th}$.

2.2. Brightness gains calculations for rectangular moderator

Using the approach described above, we can calculate the brightness of the moderator when it is illuminated from all sides. We consider two cases (Fig. 5): illumination from the left and right sides, and illumination from the top and bottom sides. In each case, we can determine the partial cold neutron intensities by calculating the corresponding neutron path lengths (s_i and b_i , respectively) for the four segments of the moderator area (shown differently shaded in Fig. 5) and for each neutron emission point P defined by the positional offset Δ with respect to the moderator center. Total cold neutron intensities $I_S(W, H)$ and $I_B(W, H)$ for the side and bottom illumination, respectively, can be obtained by integrating over the moderator height H or width W and the emission angle θ measured from the normal to the emitting surface. Detailed calculations of total cold neutron intensities are provided in Appendix A.

Since the moderator is symmetric, the intensity $I_S(W, H)$ (refer to equations A1–A11) is the same for both the left and right walls. Similarly, the intensity $I_B(W, H)$ (refer to equations A12–A22) is the same for both the bottom and top walls.

From this point forward, we will calculate the brightness gain G relative to the brightness $B(10, 10) = I(10, 10)/(4\pi \cdot 10 \times 10 \text{ cm}^2)$ of the voluminous moderator with a cross-section of $10 \times 10 \text{ cm}^2$ (that is the standard size of voluminous para-hydrogen moderators [15]) under the same illumination conditions:

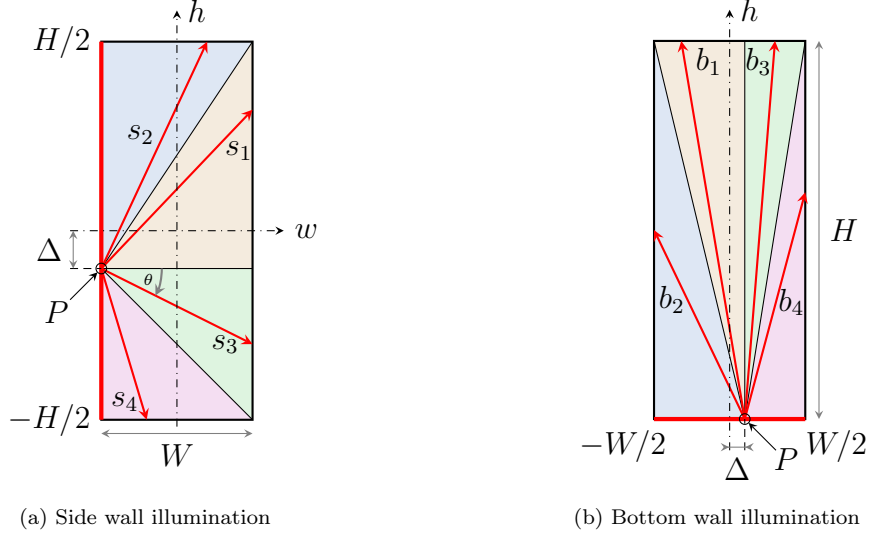


Figure 5: Illustration of infinitely thin moderator illumination

$$G_S(W, H) = \frac{B_S(W, H)}{B(10, 10)} = \frac{I_S(W, H)}{4\pi (W \times H)} \cdot \left(\frac{I(10, 10)}{4\pi \cdot 10 \times 10 \text{ cm}^2} \right)^{-1} \quad (6)$$

$$G_B(W, H) = \frac{B_B(W, H)}{B(10, 10)} = \frac{I_B(W, H)}{4\pi (W \times H)} \cdot \left(\frac{I(10, 10)}{4\pi \cdot 10 \times 10 \text{ cm}^2} \right)^{-1} \quad (7)$$

As the cold neutron intensity delivered from the moderator is proportional to the brightness of a homogeneous isotropic linear source B_{th0} that illuminates the moderator, brightness gains (6) and (7) do not depend on B_{th0} . This implies that, at a first-order approximation, any inhomogeneity in the incident thermal neutron flux, such as that arising from an unilluminated wall, does not affect the calculation of brightness gain.

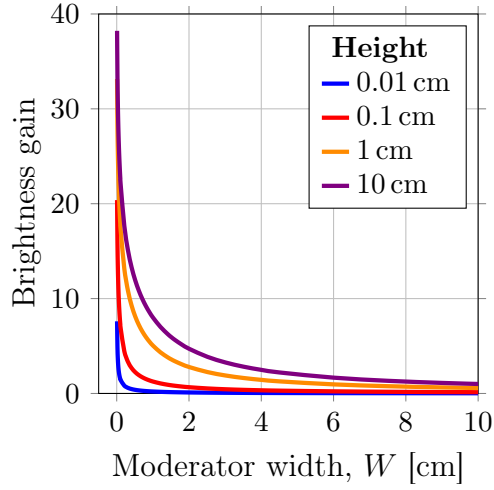
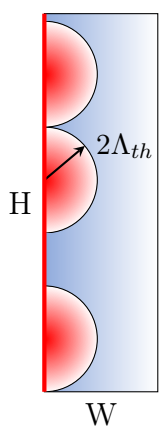
The results of the calculations for the partial brightness gains are presented in Fig. 6. It is evident from the graphs that these brightness values exhibit a significant increase as the moderator becomes narrower or as its height increases. This behavior can be explained as follows:

- Side illumination — dependence on the moderator width W (Fig. 6a).

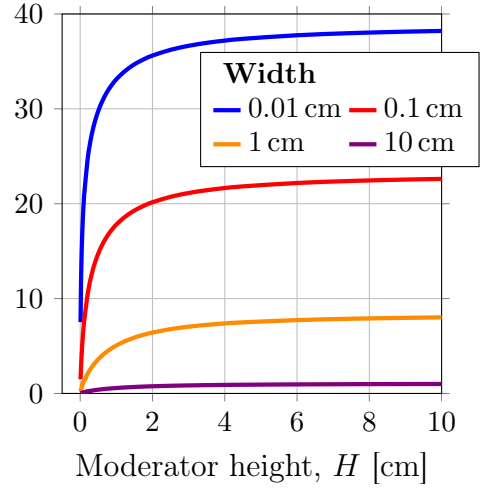
As mentioned above, approximately 95% of thermal neutrons interact with the moderator material within the $2\Lambda_{th}$ thick layer (see Fig. 3a), resulting in effective emission of cold neutrons only from this region. Therefore, as the bottom width W of the moderator exceeds $2\Lambda_{th}$, the intensity of cold neutrons does not show a significant increase. In other words, for $W > 2\Lambda_{th}$, the brightness of the cold source, which is inversely proportional to the moderator area $W \times H$ (see Eq. (6)), decreases as $1/W$ towards zero.

On the other hand, as the width W decreases from $2\Lambda_{th}$ to zero, the hyperbolic rise of $1/W$ for the cold neutron brightness is dampened by the exponential decrease of the cold neutron intensity within the $2\Lambda_{th}$ thick layer (Eq. (2)). As a result, the brightness of cold neutrons increases rather sharply for narrower moderators, but it does not diverge for $W = 0$; instead, it approaches a limiting value.

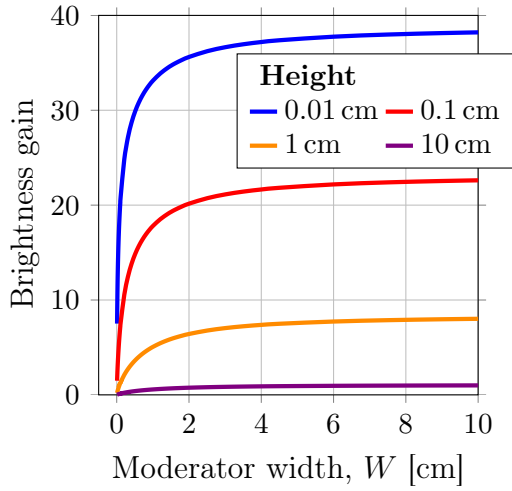
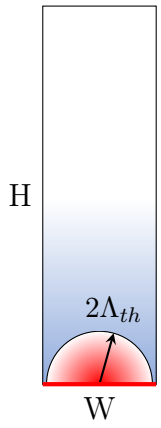
- Bottom illumination — dependence on the moderator width W (Fig. 6c).



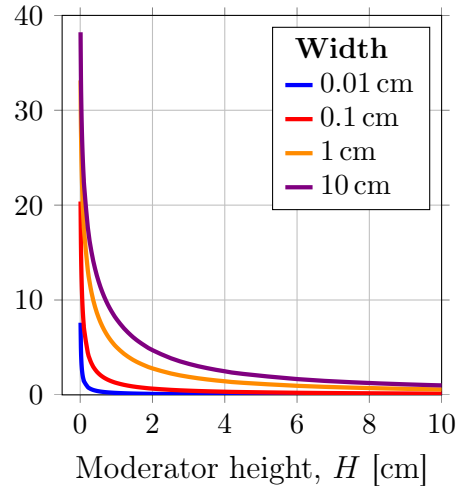
(a) Side wall illumination, various heights



(b) Side wall illumination, various widths



(c) Bottom wall illumination, various heights
(the curves are the same as in subfigure b)



(d) Bottom wall illumination, various widths (the curves are the same as in subfigure a)

Figure 6: Moderator brightness gain as a function of its dimensions for $\Lambda_{th} = 1$ cm with various illumination conditions.

Unlike to the previous case, where the change in moderator width W did not affect the size of the thermal neutron source (vertical wall in Fig. 6), in this case, it does have an impact. For large values of W , more than $2\Lambda_{th}$, the cold neutron intensity is proportional to W , as the vast majority of thermal neutrons emitted from each point on the bottom wall are converted into cold neutrons in a single collision. Therefore, the cold neutron brightness, as defined by Eq. (7), is independent of W and inversely proportional to the moderator height H . However, as the width W gradually decreases from $2\Lambda_{th}$ to zero, a portion of thermal neutrons emitted at angles $\theta \neq 0$ (i.e. not vertically) will not undergo collisions with the moderator material. This leads to a decrease in the cold neutron intensity (see Eq. (4) and Fig. 3a)

- Side illumination — dependence on the moderator height H (Fig. 6b)

The dependence of cold neutron brightness on the moderator height for the side illumination (Fig. 6b) exhibits exactly the same behavior as dependence on the moderator width for the bottom illumination (Fig. 6c). Such kind of symmetry is not surprising: in the first case, the illuminated vertical side wall plays a similar role to the illuminated horizontal wall in the case of bottom illumination.

- Bottom illumination — dependence on the moderator height H (Fig. 6d).

This dependence is but exactly the same as dependence on the moderator width for the side illumination (Fig. 6a). Now the illuminated horizontal bottom wall plays the same role as the illuminated vertical wall for the side illumination.

The total moderator brightness is obtained as the sum of left-right, $B_S(W, H)$, and top-bottom, $B_B(W, H)$ partial brightness,

$$B(W, H) = B_S(W, H) + B_B(W, H), \quad (8)$$

so that the brightness gain for fully illuminated moderator is given by

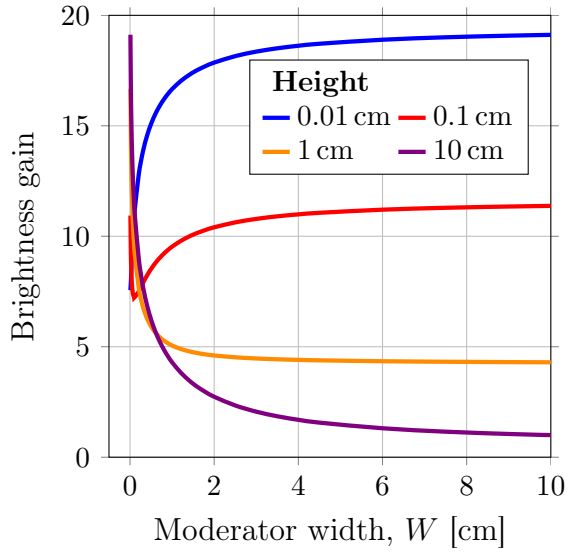
$$G(W, H) = \frac{B(W, H)}{B(10, 10)} = \frac{G_S(W, H) + G_B(W, H)}{2}. \quad (9)$$

The factor of 2 in Eq. (9) here arises from the fact that both brightness gains G_S and G_B are already normalized to the brightness $B(10, 10)$ of the voluminous moderator.

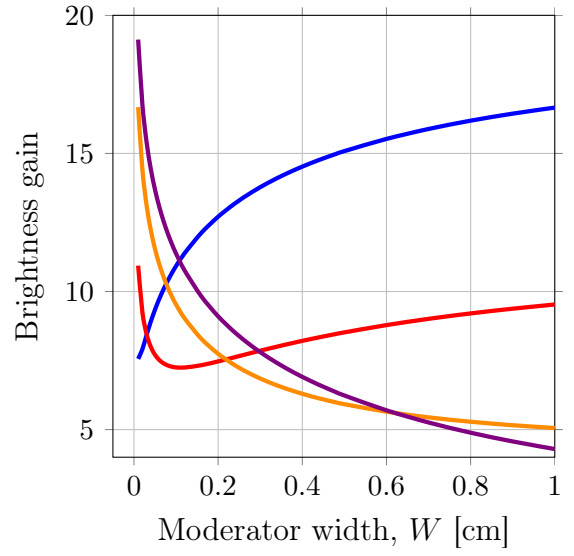
The brightness gain of fully illuminated moderator is presented in Fig. 7 (for coarse (Fig. 7a) and fine (Fig. 7b) scales). One can see that rather high gains, about 10, can be achieved for moderators with sizes of about (0.1×10) cm². Here the minimal moderator width considered is $W = 0.01$ cm, while for smaller values of W even higher brightness gain can be observed. Note the non-monotonic behavior of brightness for moderator of 0.1 cm height; the physical explanation of this fact will be given in Sect. 3.

As one can see from Fig. 8 below, there is a strong dependence of the neutron cross-section (or MFP) on the neutron energy in the region of the maximum of the thermal Maxwellian spectrum. However, as it is seen from Fig. 3, the brightness gain is larger for shorter MFPs, while characteristic features of the behavior of the brightness gain are conserved.

It is important to note that the simple summing up of the two partial brightness in Eq. (8) is valid only if the cold moderator is homogeneously illuminated from all sides. This assumption holds true in the case of heavy water thermal moderators commonly used in research reactors. However, if the cold moderator is placed in a light water moderator or in close proximity to the target of an accelerator-driven neutron source surrounded by reflectors,

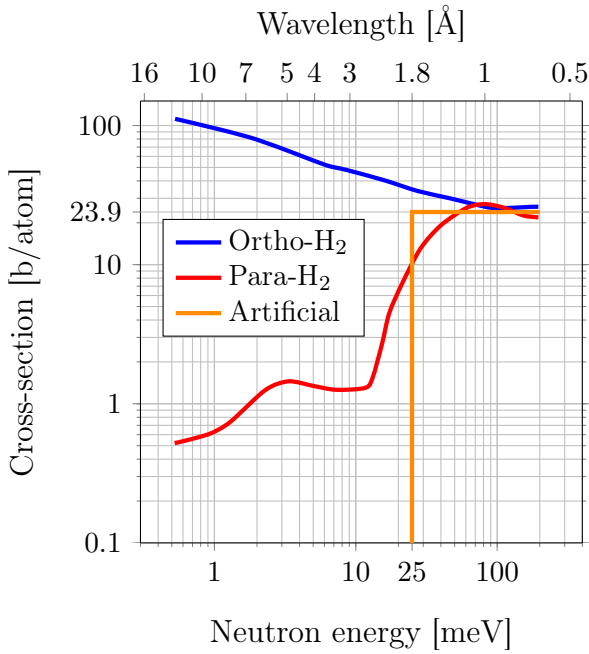


(a) Coarse scale

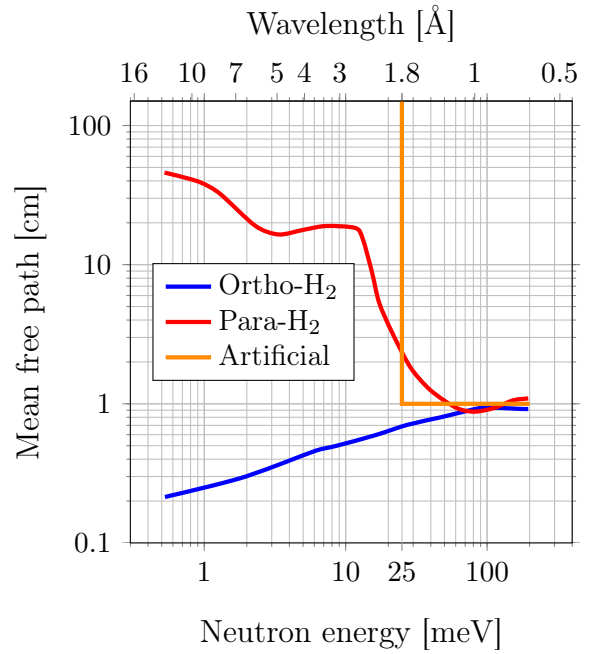


(b) Fine scale

Figure 7: Brightness gain of fully illuminated moderator for different moderator heights



(a) Cross-section.



(b) Mean free path.

Figure 8: Energy dependence of cross-section and mean free path of neutrons in ortho- and para-hydrogen at 20 K. Orange lines correspond to the artificial step-like cross-section. Recalculated from [16, figure 30 on page 367].

the illumination becomes non-homogeneous. In such cases, the summing up of the partial brightness needs to be performed with corresponding weights to account for the non-uniform illumination.

It is worth mentioning that when only one side wall of the cold moderator is illuminated the brightness gain is twice as much compared to full illumination (compare maximal gains in figures 6 and 7). However, these larger relative gains do not mean larger absolute values of cold neutron brightness.

2.3. MCNP verification

The scattering of cold neutrons in para-hydrogen is very weak: the microscopic scattering cross-section σ_s of para-hydrogen for neutrons with energies below 13 meV is only about 1 b (see Fig. 8a) that corresponds to the mean free path Λ_{th} of about 20 cm. Therefore, cold neutrons produced in the depth of the moderator volume can propagate over distance $l = 10 - 15$ cm to the moderator face without significant losses.

Analytic calculations shown above predict significant brightness gains for narrow cold moderators. To validate and further explore these findings, it is crucial to compare them with results obtained from MCNP simulations. However, there is a difference in these two approaches in calculating the intensity of the cold neutron beam. In the analytical calculations, the intensity is determined under the assumption that a single collision is sufficient to slow down thermal neutrons to cold energies. On the other hand, in MCNP simulations, the number of cold neutrons produced in the moderator from thermal neutrons is directly calculated using the scattering cross-section $\sigma(E_n)$ for para-hydrogen. This means that multiple collisions are not excluded in the MCNP simulations.

To ensure a fair comparison between our analytic calculations and MCNP simulations, we need to limit the simulations to single collisions. For this purpose, we replace the real cross-section $\sigma(E_n)$ (shown in Fig. 8a) with an artificial step-like cross-section $\sigma_{art}(E_n)$ that has a value of $\sigma_{art} = 23.9$ b ($\Lambda_{th} \approx 1$ cm) for thermal neutrons with energies $E_n \geq 25$ meV, and a value of $\sigma_{art} = 0$ for neutrons with $E_n < 25$ meV (represented by a solid orange line in Fig. 8a). Additionally, we set the energy of incident thermal neutrons to 25 meV, so that even a small energy loss due to a collision will result in the conversion of thermal neutrons to cold neutrons. The neutrons are detected by the next event estimator (f5), which is a point detector placed at a distance of $r = 100$ m from the moderator. The point detector records cold neutrons with maximal energy set to 24.99 meV emitted within the solid angle $\Delta\Omega = S/r^2$, where S is the emission surface of the moderator, given by $S = W \times H$. Since the step-like cross-section $\sigma_{art}(E_n)$ equals to zero for neutrons with energies below 25 meV, there is no absorption of cold neutrons in para-hydrogen after their conversion from thermal neutrons. This approach allows us to focus solely on the effect of single collisions on the conversion process in the MCNP simulations, enabling a direct comparison with the results obtained from the analytic calculations.

In Fig. 9 the results of the MCNP simulations are represented by black symbols² and are superimposed on the results obtained from the analytic calculations shown in Fig. 7a. The excellent agreement between the two sets of results demonstrates the accuracy and reliability of both the analytic calculations and the MCNP simulations. This strong validation allows us to confidently rely on the MCNP simulations for further analysis and investigation of neutron moderation phenomena.

²The results of MCNP calculations are consistently reported with statistical uncertainties. In cases where the error bars are not discernible, it indicates that they fall within the boundaries of the marker footprint.

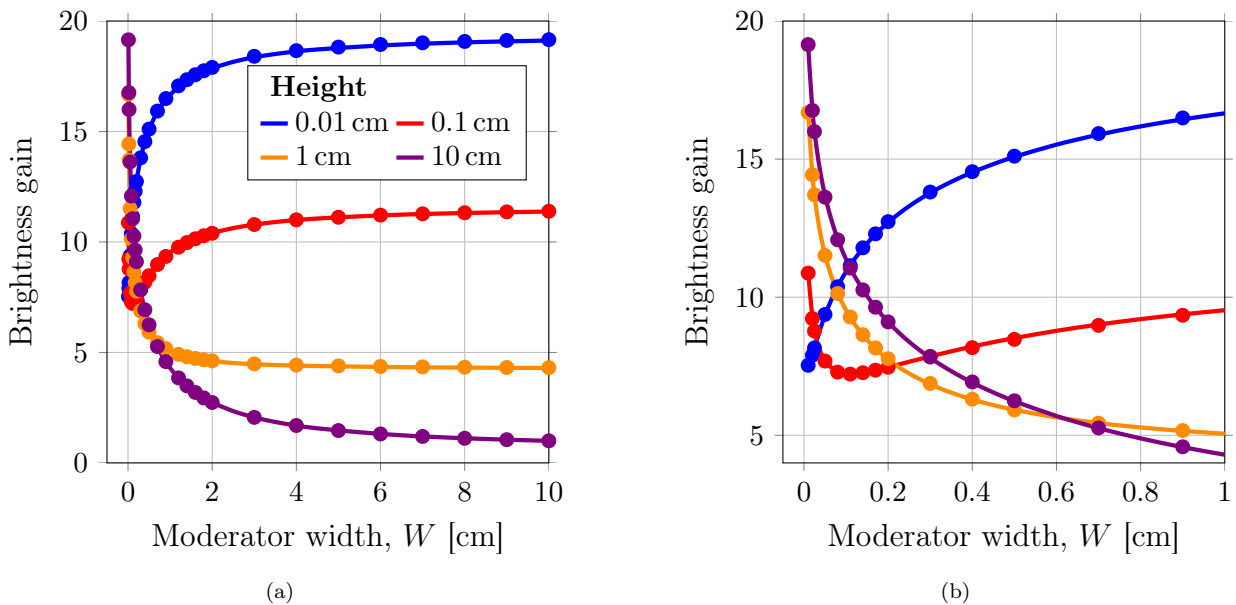


Figure 9: (a) Comparison of MCNP simulations (circles) with analytic calculations (curves) in Fig. 7; (b) Zoomed-in view of Fig. 9a for moderator widths below 1 cm.

3. What is the low-dimensionality of moderators?

Now we would like to discuss the physical question: what is the actual meaning of “low-dimensionality” in moderators that leads to a significant brightness gain? In literature, moderators with shapes such as tubes or disks that have face dimensions smaller than the voluminous moderators’ faces (typically about $10 \times 10 \text{ cm}^2$), are commonly referred to as low-dimensional moderators [4–6]. In the following discussion, we will attempt to provide a physical interpretation of the term “low dimensionality”.

Low-dimensional moderators are created by compressing the voluminous moderators in one or two directions. When considering only the dimensions of the moderator faces (height H and width W), classical voluminous moderators are geometrically 2-dimensional with the aspect ratio H/W of about 1. On other hand, the ESS-type flat moderator [6] with an elongated face is geometrically 1-dimensional with an aspect ratio considerably larger than 1, and provides significant brightness gain of about 2–3 times compared to voluminous moderator (see the point at $W = 3 \text{ cm}$ on the violet curve in Fig. 9a for illustration).

Intuitively, one could assume further similar gains of about 2–3 times, which could be obtained by the compression of moderator along its second dimension. However, MCNP simulations have shown only modest increase of 20–25 % (for neutron wavelength about 3 \AA) as shown in [5, Figure 3].

We suggest the following explanation for this effect. Note, the obtained tube-like moderator is geometrically 2-dimensional, since the ratio H/W is close to 1. Indeed, while the brightness gains are rising monotonically in the sequence “voluminous \rightarrow flat \rightarrow tube-like” moderators, their dimensionality changes non-monotonically: 2D \rightarrow 1D \rightarrow 2D. Thus, brightness gains can’t be explained solely from geometrical properties, i.e., the face dimensionality. To be considered low-dimensional in terms of moderator physics, in addition to having a high aspect ratio (being geometrically 1-dimensional), the moderator should also be low-dimensional “physically”. This physical dimension is defined by the mean free path Λ_{th} . More specifically, the physical scale is $2\Lambda_{th}$, which represents the distance beyond which there is essentially no further production of cold neutrons, because only a small number of thermal neutrons (about 5 %) can penetrate to such depths in the moderator material.

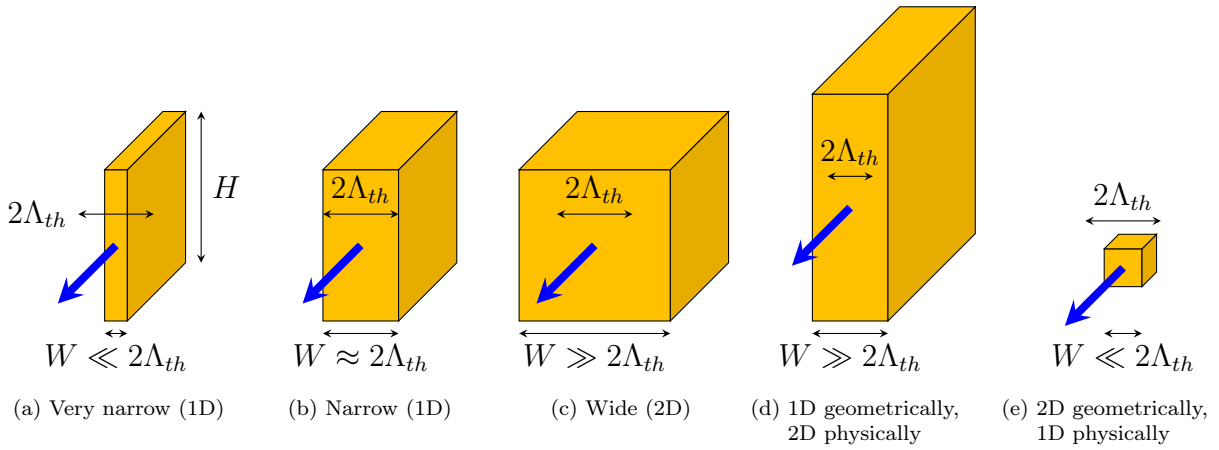


Figure 10: Classification of moderators according to their geometrical and physical dimensionality. High brightness gains are achieved only by moderators that possess both a high aspect ratio (1D geometrically) and physical narrowness.

In our discussion, moderators with a width $W \approx 2\Lambda_{th}$ are referred to as narrow moderators, while moderators with a width $W \gg 2\Lambda_{th}$ are referred to as wide moderators. Indeed, for a moderator to be considered 1-dimensional, it needs to fulfill two criteria: (a) it should have a 1-dimensional shape, meaning it is elongated in one direction and (b) it should also be “narrow” with a width $W \approx 2\Lambda_{th}$. Only moderators meeting both of these criteria, as represented in figures 10a and b, are capable of delivering a significant increase in brightness.

This situation can be conveniently represented by a “phase diagram” shown in Fig. 11, which illustrates the relationship between brightness gain and moderator width and height. Two inclined white lines represent the boundaries where moderators have a 1-dimensional geometric shape, characterised by a high aspect ratio. The green lines represent the boundaries where the moderators are considered 1-dimensional physically, being narrow in width or height.

The areas enclosed by solid lines of both colours indicate regions where high brightness gain is achieved, satisfying both geometric and physical conditions. In contrast, the large central area represents regions of low or no brightness gain. The corresponding shapes of the moderators for each area are also depicted in Fig. 11.

The curves shown in Fig. 9 correspond to the horizontal sections of Fig. 11. For example, the violet curve corresponds to the cut at the very top of the diagram ($H = 10$ cm): moderators with small W provide significant brightness gains, while moderator with $W = 10$ cm provides gain of exactly 1. Blue curve corresponds to the cut at the very bottom of the diagram ($H = 0.01$ cm): gains for moderators with small W are modest and become larger for larger W .

This allows us to explain the non-monotonic dependence of brightness gain for a moderator with height $H = 0.1$ cm at small values of width W (Fig. 9b). This effect is explored in Fig. 12 where the zoomed-in area of the region near the origin of Fig. 11 is shown. The change in the moderator width for a fixed height value corresponds to the dashed line in Fig. 12a, which represents a slice along $H = 0.1$ cm. As the moderator width, W , increases, this line traverses through 1-dimensional, then 2-dimensional, and again 1-dimensional regions, each associated with different brightness gains.

During this evolution, the shape of the moderator changes from vertically elongated to horizontally elongated (see Fig. 11); in both cases, the moderator exhibits a high brightness gain. However, in between these two extremes, when the moderator has a square shape, the brightness gain is lower as it is depicted in Fig. 12b (that is a copy of Fig. 7b and placed

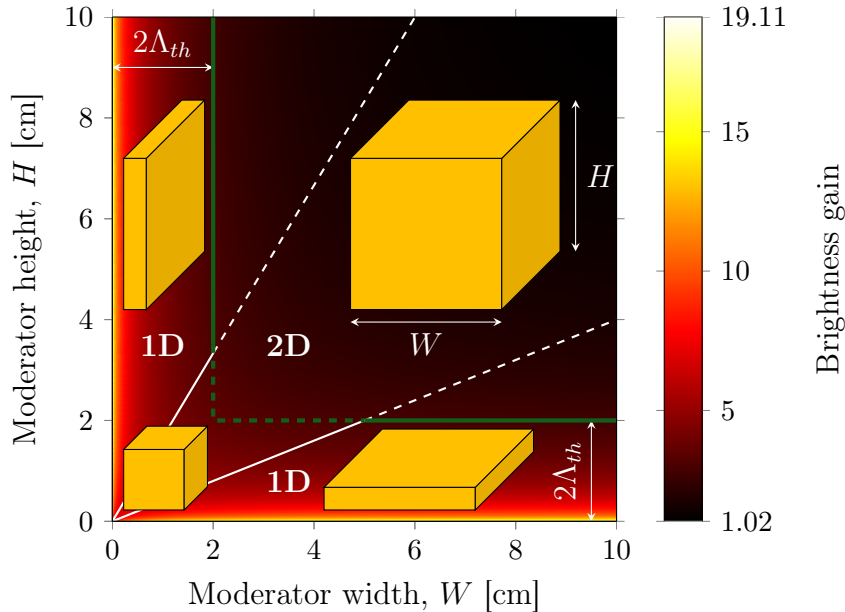


Figure 11: Brightness gain as a function of moderator width and height. The figure also includes illustrations of different moderator shapes associated with various regions of the map.

here for the reader’s convenience).

Fig. 13 exhibits the same data as Fig. 11, but plotted with respect to different coordinates. Here, instead of moderator width and height we use “physical dimension”, denoted as W/Λ_{th} , and “geometrical dimension”, represented by the aspect ratio W/H . This representation visually supports our conclusions about the physical meaning of low-dimensionality of moderators. Generally, the brightness gains are higher for lower physical dimension and high aspect ratio. If W is significantly different from H , such that both $W/H \gg 1$ and $W/H \ll 1$ cases are classified as “high” aspect ratios and correspond to horizontally or vertically elongated moderators, respectively, this difference is irrelevant for our considerations.

Note relatively low gains for aspect ratio of unity, even for physically low-dimensional moderators.

The highest possible gains are achieved when both physical and geometrical dimensions are low.

4. Real para-hydrogen moderator

Up to now, we have considered a model of a para-hydrogen moderator with the following assumptions: (a) the moderator is infinitely thin, (b) it is illuminated by a linear thermal neutron source that emits neutrons isotropically but only in the moderator plane, (c) the thermal neutrons are monochromatic with $E = 25$ meV, and (d) the step-like scattering cross-section, so that the conversion of thermal neutrons to cold neutrons takes place in a single collision with a hydrogen molecule.

In reality, moderators are of finite length and they are uniformly illuminated by thermal neutrons with Maxwellian energy distribution and the conversion to cold neutrons can involve multiple collisions — indeed, neither of the above-mentioned assumptions holds. Now, we will proceed by consequently discarding these assumptions in order to perform calculations involving a real moderator.

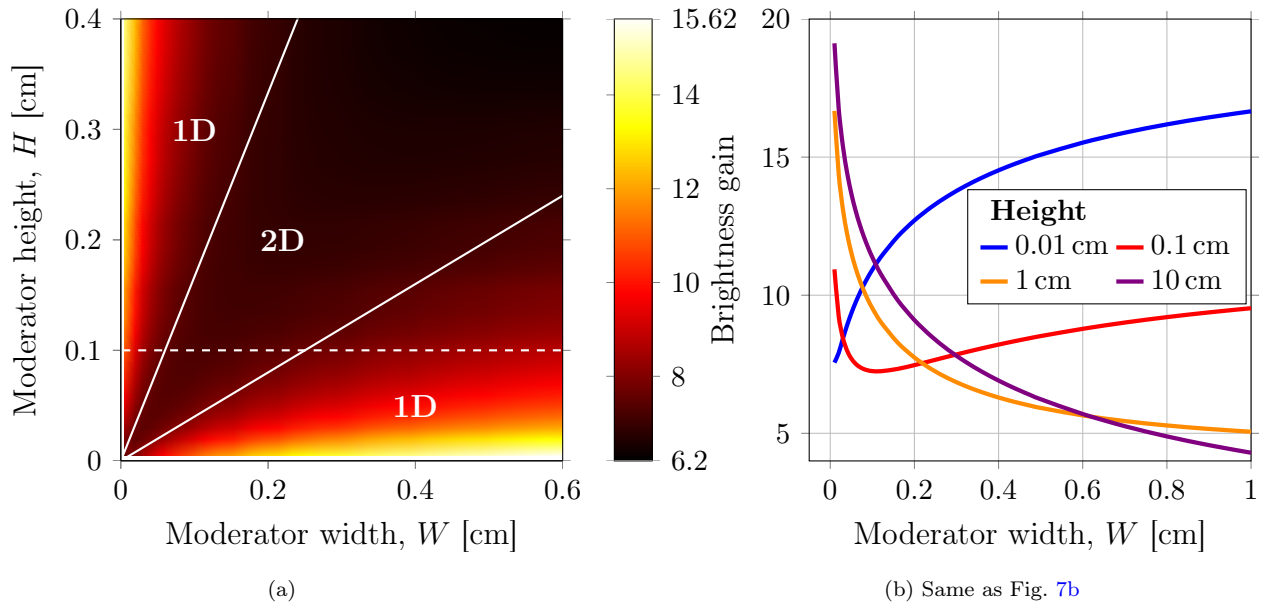


Figure 12: (a) Zoomed-in area of the region near the origin of Fig. 11. White dashed line corresponds to the $H=0.1$ cm curve in the [b](#) subfigure. (b) Brightness gain as a function of moderator width (a copy of Fig. 7b). Red curve corresponds to the cut discussed in the text.

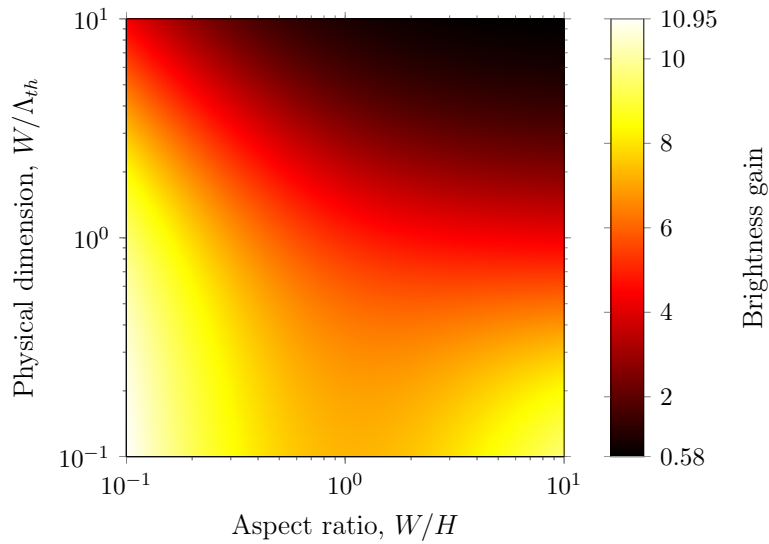


Figure 13: Brightness gain as a function of physical dimension and aspect ratio.

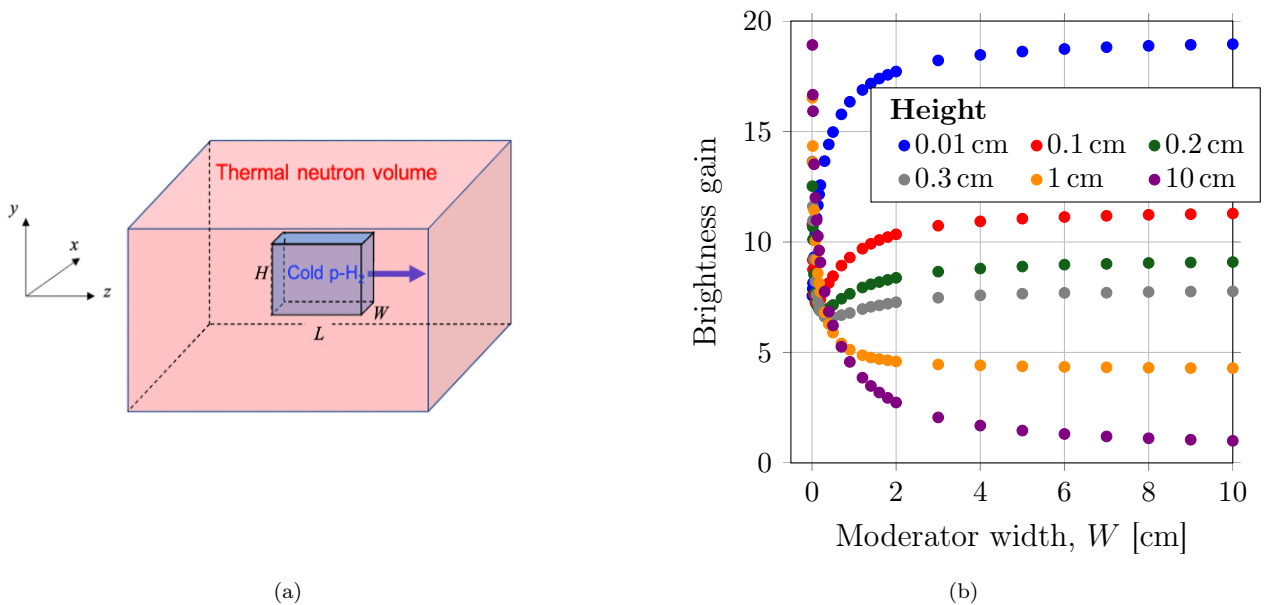


Figure 14: (a) Para-hydrogen moderator in the thermal neutron volume created by a large thermal moderator (not shown). Blue arrow shows the direction of the emitted cold neutron beam. (b) Brightness gain for the cold moderator illuminated from left, right, top and bottom surfaces as calculated with MCNP.

4.1. Transition from infinitely thin to finite length moderator.

Let's consider a para-hydrogen moderator that is immersed in a thermal neutron volume created by thermal moderator, as shown in Fig. 14a. In this configuration, all four surfaces of the para-hydrogen moderator — left, right, top, and bottom (with the neglect of illumination on the front and back faces) — are exposed to thermal neutrons and indeed can be considered as emitters of thermal neutrons.

To analyze this configuration, we can divide the para-hydrogen moderator into thin slices, similar to what we discussed earlier. Each slice emits cold neutrons along the length L of the moderator towards the point detector. Since cold neutrons are now generated in the volume $W \times H \times L$, the brightness gain is calculated relative to the volume of the moderator, which has dimensions of $(10 \times 10 \times L) \text{ cm}^3$, with L representing the length of the moderator.

Fig. 14b illustrates the results of MCNP simulations where the thermal neutron source is placed along the perimeter of an infinitely thin para-hydrogen slices and neutrons are emitted isotropically in the (x, y) plane. As expected, there is no difference between the brightness gain in this configuration and that of a single slice, as shown in Fig. 9.

4.2. Transition to out-of-plane illumination

Now we will extend our analysis to the case where each of infinitely thin thermal neutron sources placed along the perimeter of each of the para-hydrogen slices (which altogether constitute the finite length moderator) emits neutrons isotropically in space rather than in the (x, y) plane as it was considered above. Indeed, now the production of cold neutrons from any particular thin thermal neutron source occurs not solely within the corresponding thin slice but within a broader layer with a thickness of about $4\Lambda_{th}$ in the z -direction, where 95% of the cold neutrons are born.

The dependence of brightness gains on the width and height of the moderator for out-of-plane illumination is illustrated in Fig. 15. This figure demonstrates that the brightness gain is approximately three times greater when compared to the results obtained for in-plane illumination, as shown in Fig. 14b. To understand the reasons for the greater brightness gain in the out-of-plane case, it is important to note that the origin of thermal neutrons (the

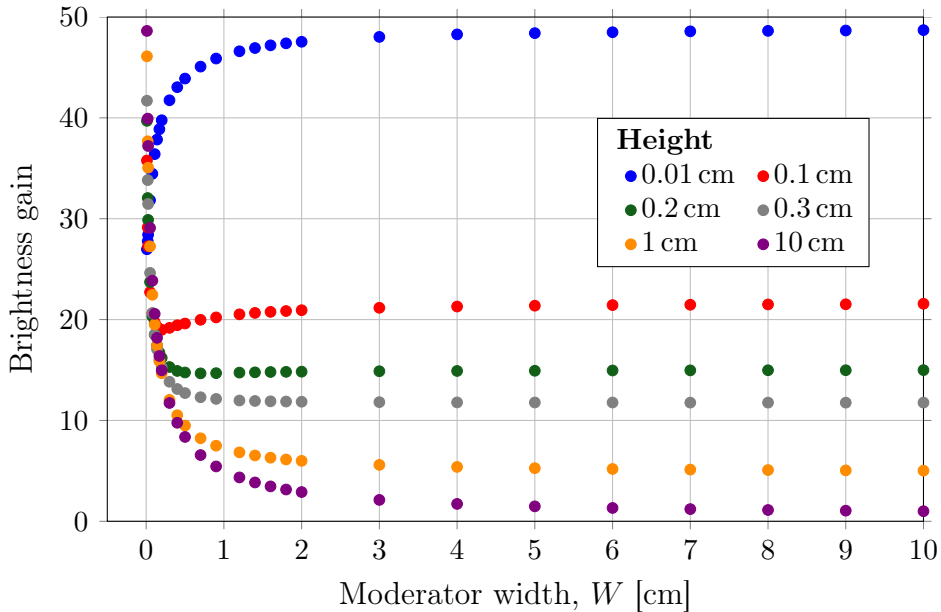


Figure 15: Brightness gains for the out-of-plane illumination.

perimeter of the moderator slice in both cases) is not relevant for calculating the brightness gain. Instead, what matters is the location where these neutrons convert into cold neutrons.

Let's consider a simplified scenario where thermal neutrons are emitted from a single point (Fig. 16). In the in-plane case, the region where 95% of the cold neutrons are born can be described as a semicircle with a radius of $2\Lambda_{th}$. In the out-of-plane case, this region becomes a hemisphere with the same radius and can be represented as a combination of smaller semicircles normal to the z -axis and offset from each other along this axis (as shown in Fig. 16b). For these offset semicircles, the region of cold neutron origination is compressed, effectively reducing the mean free path of the thermal neutrons. However, as we already know, the brightness gain increases with a decrease in the mean free path (as shown in Fig. 3b). Therefore, the gain will be greater for all these offset semicircles compared to the in-plane case. Since the overall brightness gain is the sum of the gains for each of these semicircles, the total brightness gain in the out-of-plane case is greater than in the in-plane case.

It is also possible to estimate the brightness gain analytically in the out-of-plane case by following a similar approach as in the two-dimensional case described in Sect. 2. This involves applying an additional integration over the out-of-plane angle.

4.3. Transition from monochromatic to Maxwellian spectrum illumination

Now, we will shift from illuminating the moderator with a monochromatic spectrum to using a Maxwellian spectrum with temperature 300 K. The results of the calculations are presented in Fig. 17. As seen in this figure, when compared to Fig. 15, we observe a significant reduction in brightness gains, approximately by a factor of 3, upon such replacement.

To explain this effect, we should note that up until now, our focus has been on the process of slowing down thermal neutrons in the para-hydrogen moderator, assuming a single collision as the sole mechanism. This was achieved by utilizing an artificial step-like neutron scattering cross-section with a threshold at 25 meV (see Fig. 8) and a monochromatic neutron spectrum with the same energy. However, neutrons with sufficiently high energies present in the incident Maxwellian spectrum are, in principle, capable of undergoing two or more collisions within the moderator before their energy decreases to less than 25 meV,

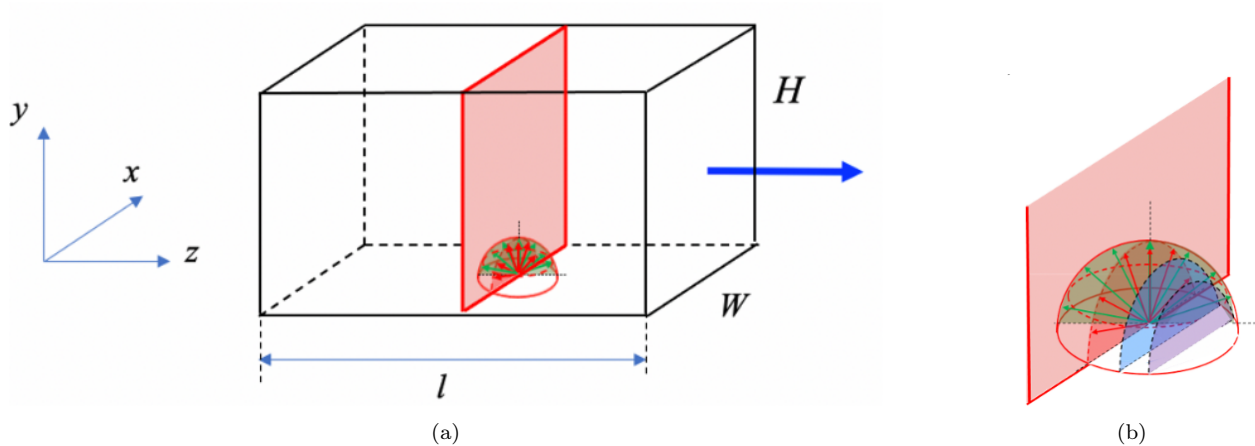


Figure 16: Out-of-plane illumination of cold moderator by an infinitely thin thermal neutron source placed along the perimeter of the para-hydrogen slice. (a) The red and green arrows indicate the directions of thermal neutron illumination in the (x, y) and (y, z) planes, respectively; the blue arrow represents the direction of the outgoing cold neutron beam towards the neutron optical system, typically a neutron guide. (b) The zoomed-in view: a hemisphere can be represented as a combination of smaller semicircles normal to the z -axis and offset from each along it

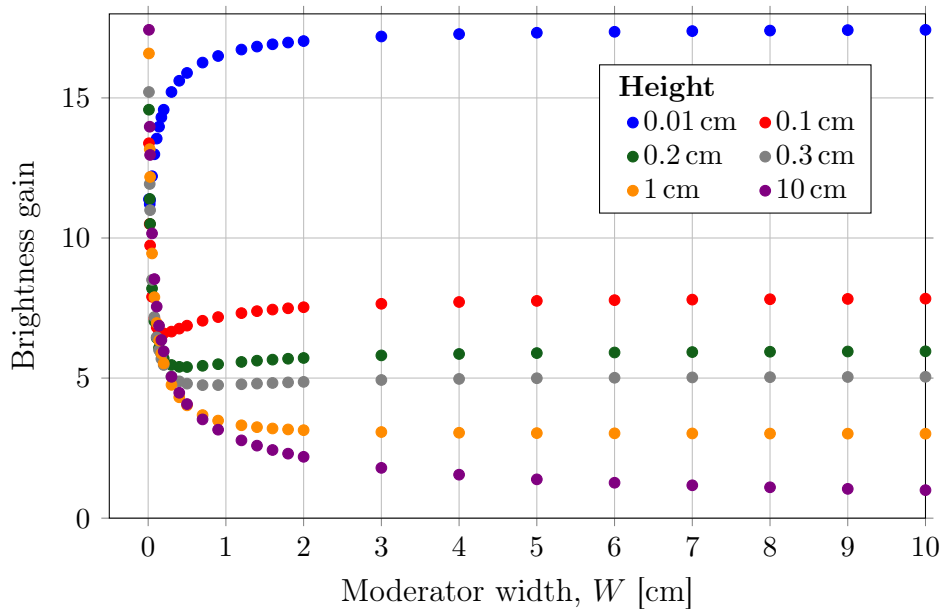


Figure 17: Brightness gains calculated for Maxwellian spectrum illumination and artificial neutron scattering cross-section (see Fig. 8a).

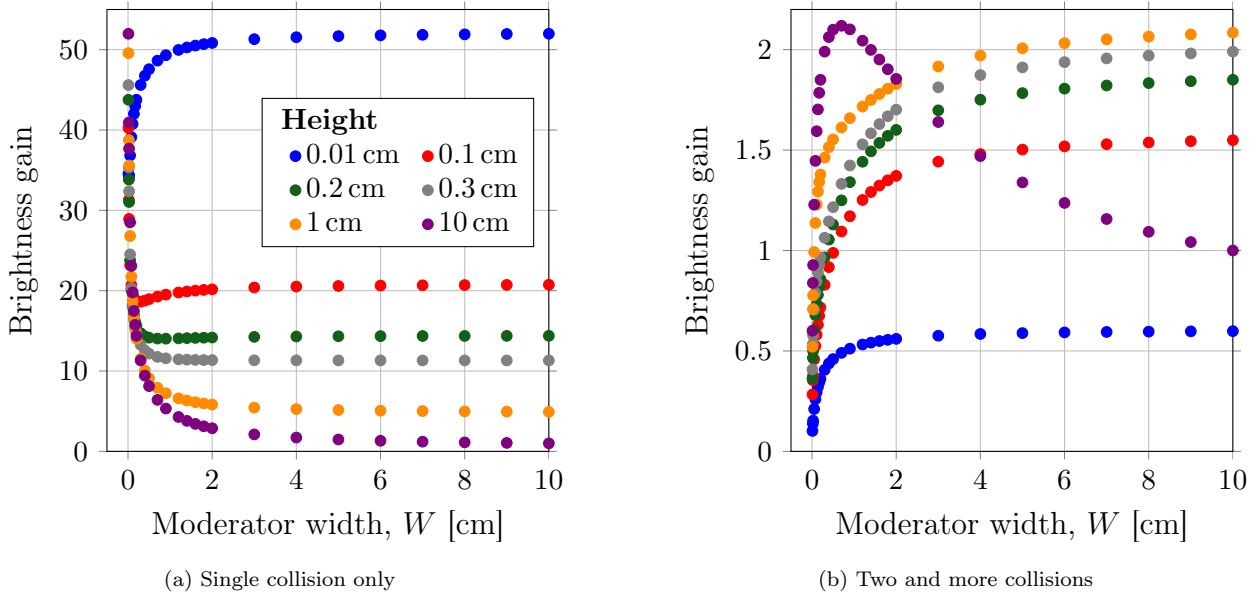


Figure 18: Decomposition of brightness gains shown in Fig. 17 on different number of collisions

allowing them to exit.

Fig. 18 illustrates the breakdown of the data presented in Fig. 17, categorized by the number of collisions. It's important to note that Fig. 18a, displaying the brightness gains of cold neutrons generated through a one-collision process, closely resembles Fig. 15: this indicates minimal difference between monochromatic and Maxwellian spectral illuminations in this particular scenario.

Now we explore Fig. 18b, where gains for multiple collision process are shown in dependence of moderator width. Let's start by analyzing the curves that relate to moderators with smaller heights. For the multiple collision process to be effective, the para-hydrogen volume surrounding the initial collision site must be significantly larger than a sphere with a radius of $2\Lambda_{th}$, because after the first collision the slowed down neutrons are scattered isotropically in all directions (in 4π). In other words, the moderator dimensions in all directions should be much greater than $2\Lambda_{th}$ to ensure sufficient volume for multiple collision events.

Indeed, for narrow moderators with dimensions $W \ll H$ and $W \ll L$, where H and L are much larger than $2\Lambda_{th}$, the probability of a second collision event is relatively small. This is because the second collision is mainly possible for neutrons that are scattered along the large surfaces of the moderator, which corresponds to a relatively small solid angle of about $4WL/H^2$. For this reason, the brightness rapidly decreases as the width approaches zero.

On the other hand, in wide moderators where all 3 dimensions W , H , and L are much larger than $2\Lambda_{th}$, the probability of multiple collisions (two or more) is almost unity due to a large volume available for neutron scattering and subsequent collisions. These can be interpreted as a single quasi-collision with an increased mean free path. The entire previously developed theory regarding brightness enhancement with a reduction in moderator width remains applicable to this quasi-collision scenario, predicting an increase in brightness. This observation aligns with the violet curve shown in Fig. 18b. However, at small widths, less than 0.5 cm, when two collisions no longer remain assured, the scenario reverts to what was described earlier, resulting in a decrease in brightness. Therefore, the scattering of thermal neutrons with energies less than 30 meV on para-hydrogen molecules is primarily a single collision process: these neutrons experience a reduction of approximately 15 meV in their kinetic energy during the initial collision. Subsequently, due to the diminishing scattering cross-section for neutrons possessing energies below 15 meV, the likelihood of undergoing a

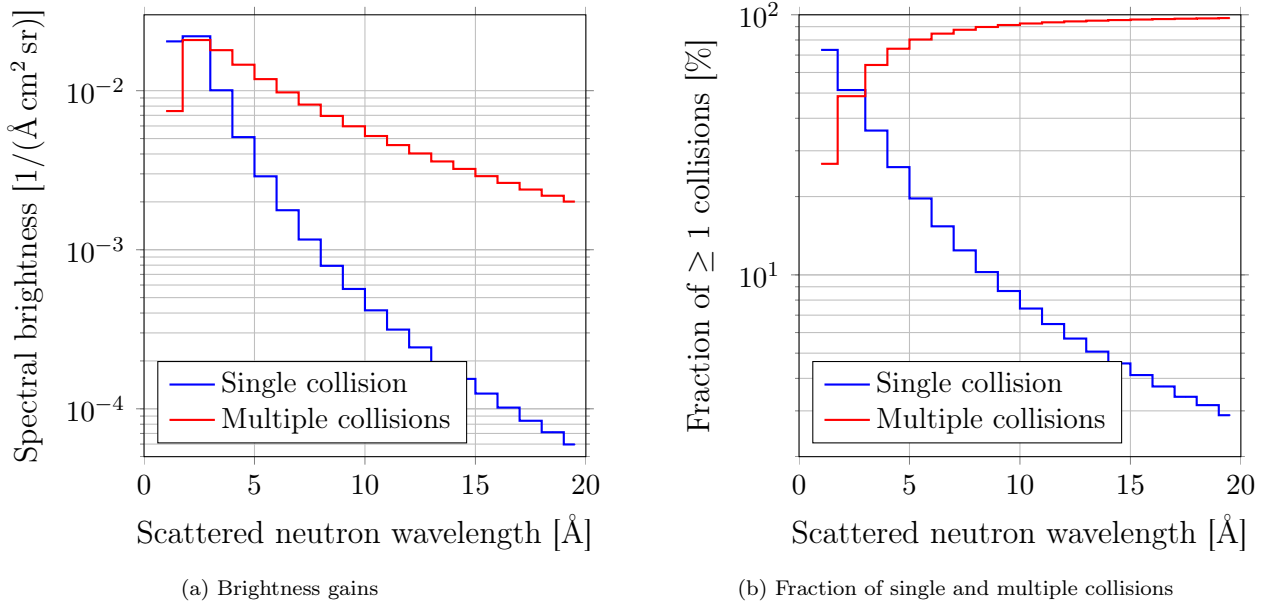


Figure 19: Wavelength dependence of brightness gains and fractions of single and multiple collisions for voluminous $10 \times 10 \text{ cm}^2$ moderator, calculated for Maxwellian spectrum illumination and artificial neutron scattering cross-section (see Fig. 8a).

second collision becomes negligible.

In this way, when illuminated by a Maxwellian spectrum, a large $(10 \times 10 \times 10) \text{ cm}^3$ moderator is capable of producing cold neutrons through both single-collision and multiple-collision processes. As the moderator size decreases, the single-collision process leads to an increase in brightness, while the multiple-collision process results in a decrease. With an increase in the moderator's size, the multiple-collision process begins to dominate, leading to an increase in the absolute brightness of the large moderator. Consequently, this leads to a reduction in the relative gain of the thin moderator (compare Fig. 15 and Fig. 17).

The expected magnitude of this reduction can be estimated using the results of MCNP calculations for the wavelength dependencies of the brightnesses and the fractions of single and multiple collisions. These calculations were performed for high-aspect ratio $(0.01 \times 10) \text{ cm}^2$ and voluminous $10 \times 10 \text{ cm}^2$ moderators, and the outcomes are presented in Figures 19 and 20, respectively.

The reduction in gain factor is directly related to the share of single-collision process in the total production of cold neutrons in the voluminous moderator. This share can be deduced from Fig. 20b by integrating over the whole spectrum with respect to the spectral brightness (Fig. 20a). Apparently this share accounts for approximately 25% of all the cold neutrons. From here, one can roughly estimate the brightness gain reduction factor as 4, which would have led to a gain factor of about 12.5 for the $(0.01 \times 10) \text{ cm}^2$ moderator, instead of the observed value of 17 (see Fig. 15 and Fig. 17). However, these considerations do not take into account that some cold neutrons, produced by multiple collisions in the voluminous moderator, are not completely lost with the decrease of the moderator size. Instead, some of them undergo only single collision in a smaller moderator and contribute to the final count of single-collision produced neutron, thus increasing the gain factors from 12.5 to 17.

4.4. Transition from step-like cross-section to real cross-section of para-hydrogen

In the final phase, we replace the artificial neutron scattering cross-section with a real para-hydrogen cross-section at 20 K (hpara.20t [17, 18]). This substitution results in an

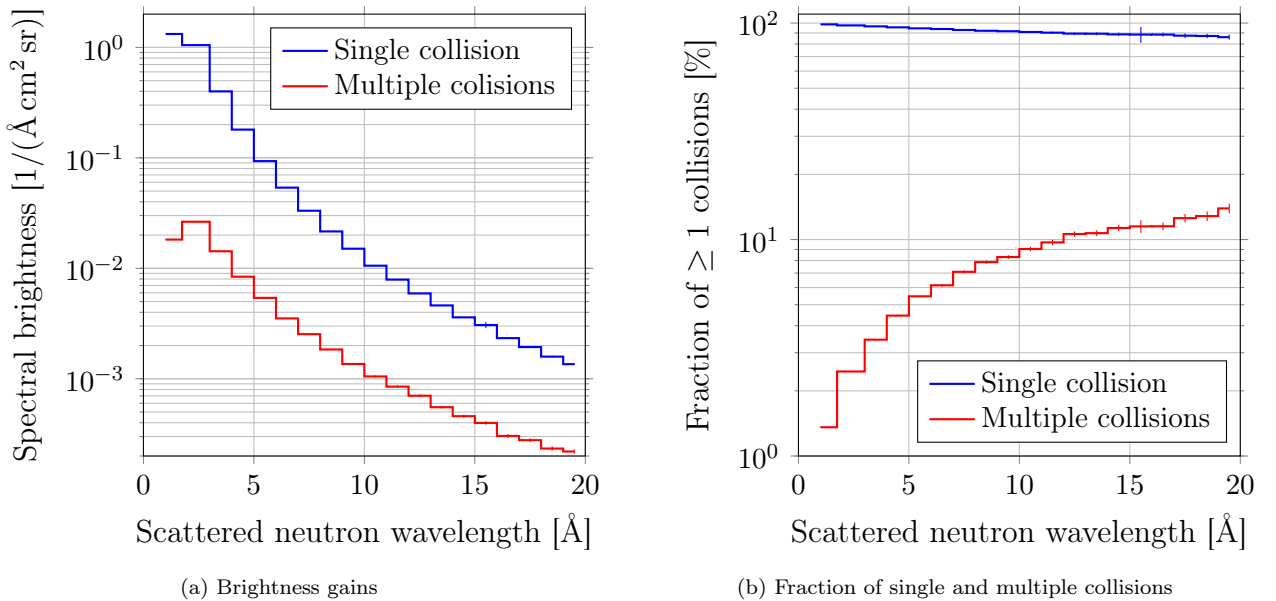


Figure 20: Wavelength dependence of brightness gains and fractions of single and multiple collisions for voluminous (0.01×10) cm^2 moderator, calculated for Maxwellian spectrum illumination and artificial neutron scattering cross-section (see Fig. 8a).

additional reduction in the brightness gain, approximately by a factor of 1.5, which varies depending on the moderator width (Fig. 21).

To elucidate this effect, we will adopt a similar method as in the preceding paragraph and break down the gains based on the number of collisions, as shown in Fig. 22. Comparing the gains obtained from single collisions (Fig. 22a) with those presented in Fig. 18a, we can observe a reduction of approximately 2.5 times. This is mainly attributed to the fact that in these processes neutrons with lower energies are involved, for which the MFP at 25 meV in the previously used step-like cross-section was 1 cm, while in the currently used real cross-section the MFP is about 2 cm (see Fig. 8b). However, as demonstrated in analytical calculations (see Fig. 3), for longer MFPs the relative brightness gains when compressing the moderator are smaller, as observed here.

Regarding the multiple-collision processes (see Fig. 18b and 22b) involving neutrons with higher energies, the MFPs for both step-like and real cross-sections are nearly identical for these neutrons, that results in the similarity between the patterns shown in these figures. Considering the proportions of both processes in the production of cold neutrons, and accounting for the reduced contributions of neutrons with longer wavelengths, we observe that for the voluminous moderator, the single-collision process contributes to around 60% of the cold neutron production, while for a narrow high-aspect ratio moderator, this contribution is about 100% (Fig. 23b). As a result, it is expected that the final brightness gains for smaller moderator sizes will be approximately 1.6 times lower compared to the gains obtained from a model solely based on the single-collision process. This is consistent with the comparison of brightness gains between Fig. 17 and Fig. 21, where, for example, the maximal gains for $H = 0.01$ cm are 17 and 11, respectively.

5. Cold neutron spectrum emitted from low-dimensional para-hydrogen moderators

The change in relative contributions from single- and multiple-collision processes, which depends on the moderator width as described in the previous section, should clearly influence

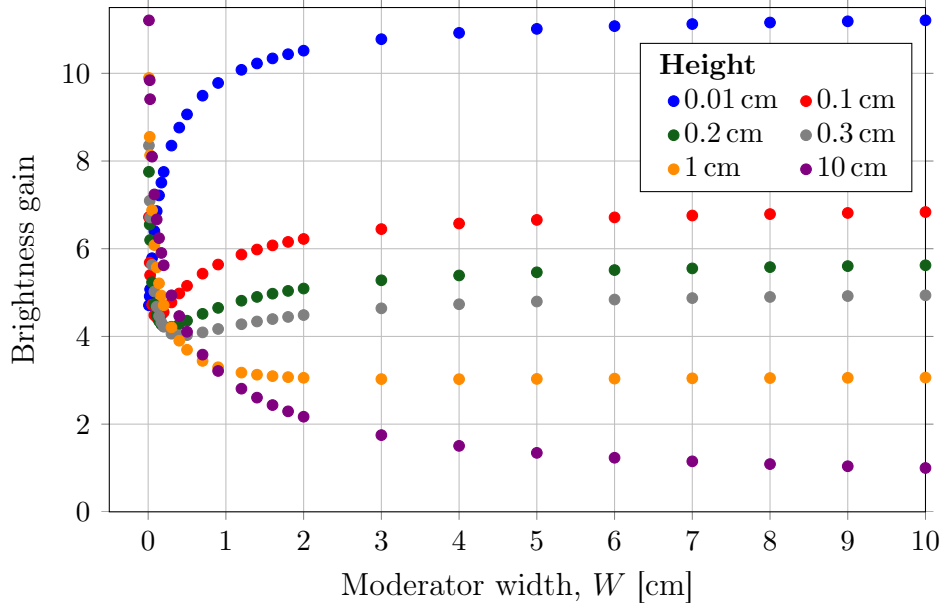


Figure 21: Brightness gains calculated for Maxwellian spectrum illumination and real para-hydrogen cross-section.

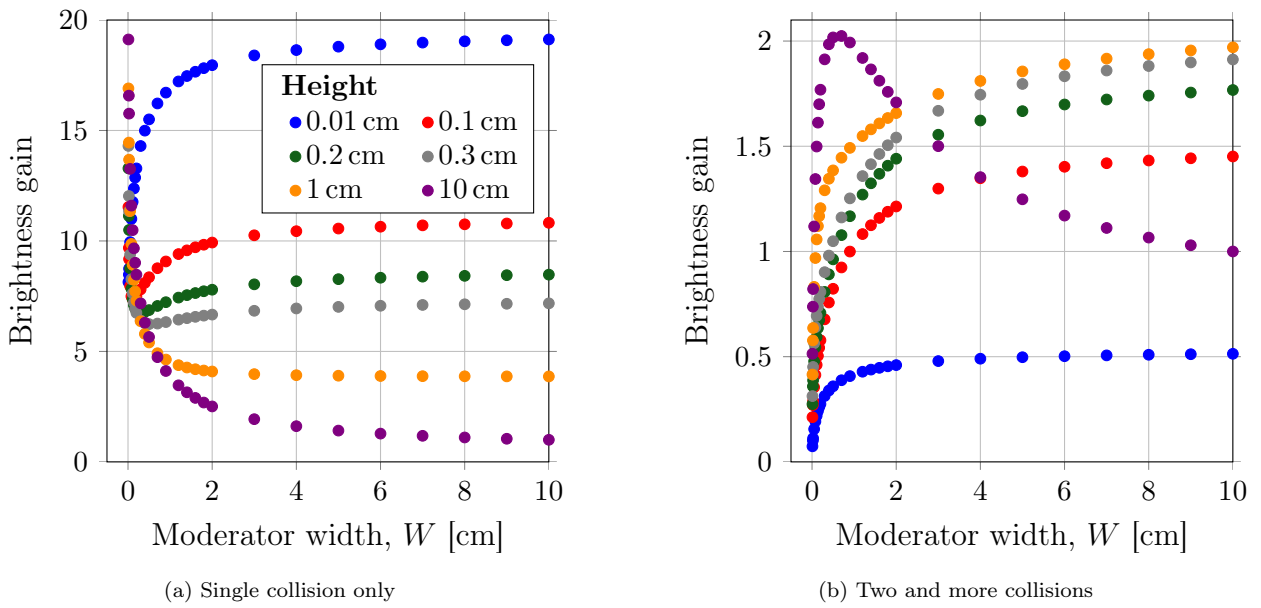


Figure 22: Decomposition of brightness gains shown in Fig. 21 on different number of collisions

the spectrum of cold neutrons emitted from such a moderator. Examples of such spectra for a voluminous $10 \times 10 \text{ cm}^2$ and a high-aspect ratio $(0.01 \times 10) \text{ cm}^2$ moderators are presented in Fig. 23 and Fig. 24, respectively, where the incident Maxwell spectrum is also depicted. The corresponding curve is artificially scaled to highlight the difference in shape between the thermal and cold neutron spectra. The Maxwell spectrum used here is actually the intensity spectrum calculated by scoring neutrons using the surface crossing estimator (f1).

Here it is important to note that the moderation process in para-hydrogen differs fundamentally from the one observed in conventional neutron moderators. In conventional moderators, high-energy neutrons are slowing down by undergoing a series of successive collisions with the moderator atoms, with each collision reducing the neutron’s energy by an average factor of e (the slowing down process). At the final stage, when neutron energy approaches the average kinetic energy of the moderator atoms, neutrons undergo further multiple collisions facilitating the exchange of kinetic energy between the neutrons and the moderator atoms till the probability of down-scattering and up-scattering become similar, so that neutrons become “thermalized”.

In para-hydrogen, the main mechanism for neutron energy loss at the final stage is not thermalization, but rather the slowing down because of the transition between rotational energy levels of the H_2 molecule, which are separated by 14.7 meV [19] (this transition is known as the para-to-ortho transition).

The fact that a neutron loses an entire 14.7 meV in a single collision with para-hydrogen molecules makes the thermal-to-cold conversion of neutrons with $E < 30 \text{ meV}$ primarily a single-collision process. Particularly, neutrons with energies in the range of $15\text{--}30 \text{ meV}$, where the maximum of the incident Maxwellian spectrum is located, essentially undergo the single-collision process, because their final kinetic energy is less than 15 meV and scattering cross-section for such neutrons is very small. Hence, the spectrum of cold neutrons exiting the para-hydrogen moderator is significantly depleted of neutrons with energies $E > 30 \text{ meV}$ ($\lambda < 1.7 \text{ \AA}$), the energy of these neutrons decreases to around 15 meV ($\lambda \approx 2.3 \text{ \AA}$), where the maximum of the neutron spectrum is anticipated to be located. These considerations are confirmed by the spectra shown in Fig. 23a and Fig. 24a (red curves), where the incident Maxwellian spectra are depicted as black curves for illustration.

Thus, in low-dimensional para-hydrogen moderators of small width, where the single-scattering process dominates, the Maxwellian spectrum observed in the outgoing neutron beam does not stem from the thermalization process typically observed in ortho-hydrogen or D_2 moderators. Instead, it is a “replica” of the Maxwellian spectrum of the incident neutrons, but with a shift towards lower energies.

6. Cold neutron source utilising assembly of low-dimensional moderators

6.1. Neutron source concept

As discussed above, narrow high-aspect ratio moderators exhibit a significant increase in brightness compared to wider voluminous moderators. Moderators with enhanced brightness are particularly advantageous for brightness-hungry instruments such as reflectometers or small-angle neutron scattering (SANS) diffractometers, where high Q-resolution requires well-collimated neutron beams. In such cases, the brightness gain directly contributes to the intensity at the sample [12].

However, this enhanced brightness comes at the expense of reduced intensity of emitted cold neutron beams due to the reduced moderator volume. Indeed, these small yet bright moderators are not as beneficial for intensity-hungry instruments with relaxed Q-resolution requirements, e.g. like neutron spin echo (NSE) or fundamental physics instruments, as they produce fewer neutrons compared to conventional voluminous moderators, albeit less bright.

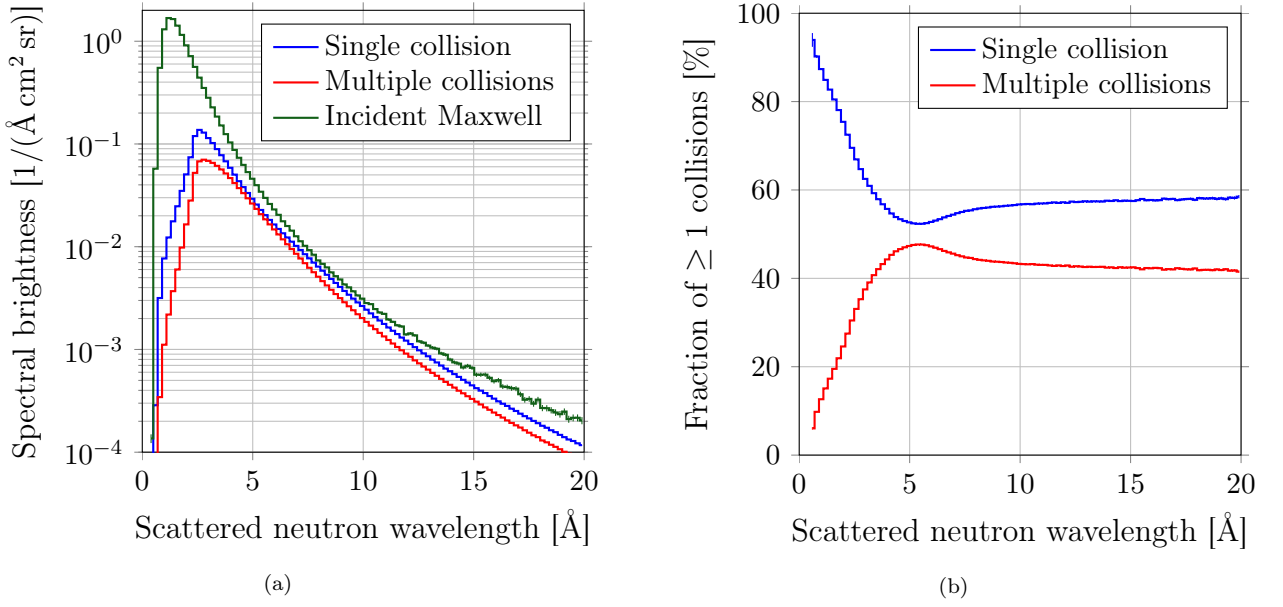


Figure 23: (a) Wavelength spectra of neutrons produced by single and multiple collisions processes in a voluminous moderator of $10 \times 10 \text{ cm}^2$. Black curve is for illustration purpose only, not to scale. (b) Fractions of neutrons corresponding to these processes for each wavelength bin.

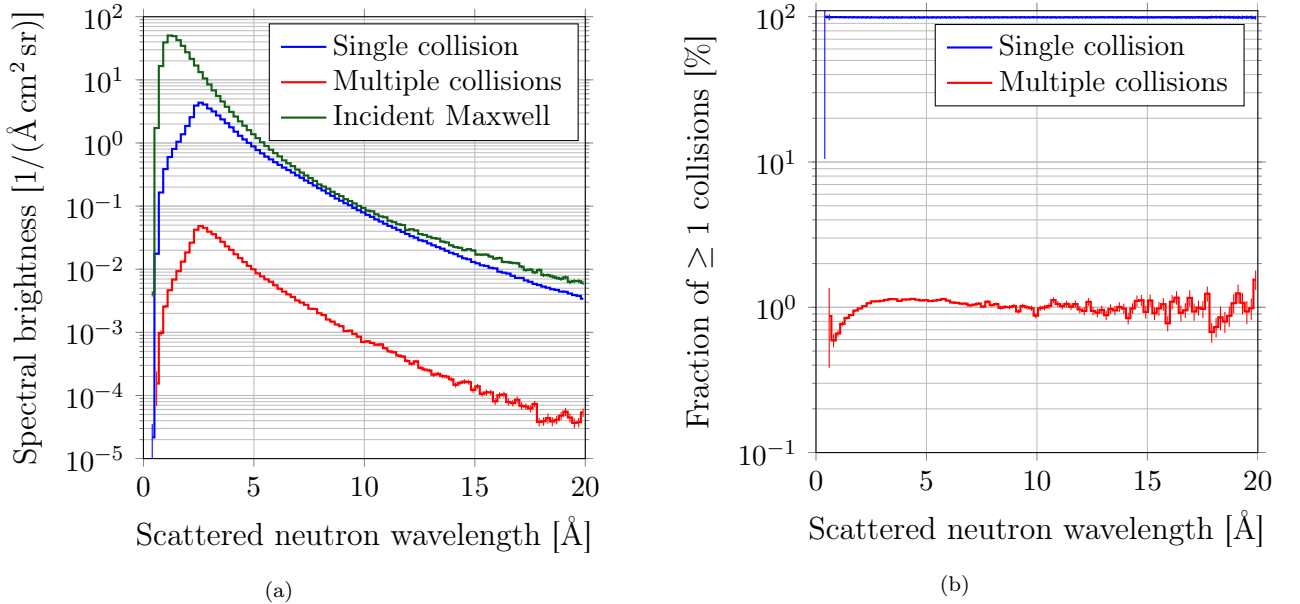


Figure 24: (a) Wavelength spectra of neutrons produced by single and multiple collisions processes in a high-aspect ratio moderator of $(0.01 \times 10) \text{ cm}^2$. Black curve is for illustration purpose only, not to scale. (b) Fractions of neutrons corresponding to these processes for each wavelength bin.

In reference [11], an analysis was conducted to investigate how moderator size affects the performance of neutron scattering instruments. It was demonstrated that the best performance is achieved with a moderator size not smaller than D_{min} , which is instrument-specific. Using smaller moderators, though with significantly enhanced brightness, leads nevertheless to the degradation of instrument performance. Such moderators under-illuminate the entrance of neutron guides that have a larger or equal cross-section compared to the moderator size. This can lead to irregularities in the structure of the outgoing beam divergence, particularly observed in the case of reflectometer HERITAGE. To address this issue, a combination of a cold moderator and a neutron guide of the same size (3 cm) has required the use of a multichannel neutron guide as a partial solution [14]. On the other hand, larger moderators ensure full illumination of the neutron guide entrance, although they provide lower beam brightness. Therefore, while larger moderators are beneficial for intensity-hungry instruments, they may result in poorer performance for brightness-hungry instruments.

Indeed, achieving both large moderator size and high brightness is highly desirable. One possible approach is to increase the neutron beam intensity by stacking multiple moderators adjacent to each other. However, it is important to consider that, as demonstrated earlier, the effective production of cold neutrons primarily occurs in the vicinity of the moderator surfaces that are illuminated by thermal neutrons. Since neighboring moderators can shadow each other, certain surfaces may not be illuminated to the same extent as in the case of a single moderator discussed earlier.

Let us consider two narrow moderators with brightnesses $B_1 = I_1/W$ (here we neglect the factor π (solid angle) as it is inconsequential to our current discussion). If these moderators are in close contact (Fig. 25a), the surfaces of the narrow moderators that are in contact are not directly illuminated by thermal neutrons; instead, they are shadowed by the adjacent moderator. Consequently, the intensity I'_1 of the cold neutron beam produced in the shadowed moderator is reduced compared to the intensity I_1 of the fully illuminated single moderator. As a result, the average brightness B_{tot} of the moderator assembly also decreases:

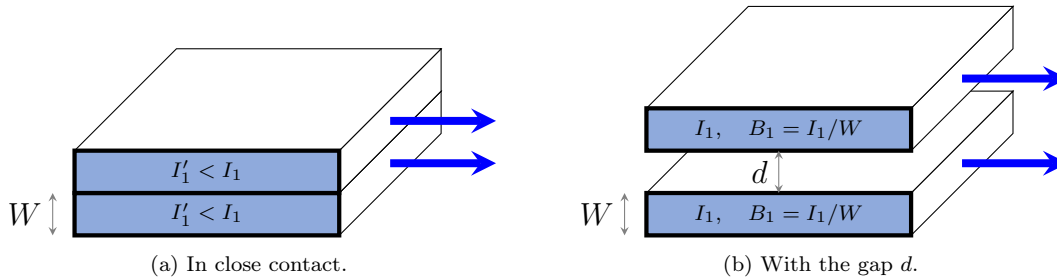


Figure 25: Arrangements of two 1-dimensional adjacent moderators. Blue arrows depict the outgoing cold neutron beam.

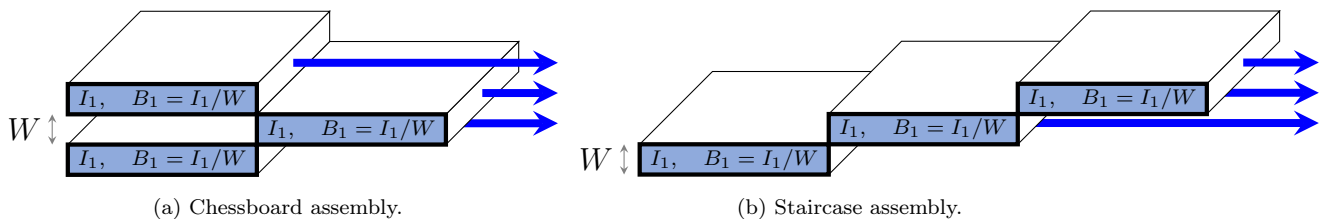


Figure 26: Assemblies of narrow moderators arranged like steps in chessboard and staircase assemblies. Blue arrows depict the outgoing cold neutron beam.

$$B_{tot} \neq \frac{2I_1'}{2W} < B_1 \quad (10)$$

Actually, the stack of N moderators is equivalent to the moderator with width $N \times W$ which brightness is reduced compared to that of a single moderator (as shown in Fig. 7). For example, within a stack of 10 narrow (0.3×10) cm² moderators, each could potentially provide a brightness of 8 (relative to the brightness of a 10×10 cm² moderator) if considered individually. However, the average brightness gain of the moderator stack will be only around 2, equivalent to that of a single 3 cm wide moderator (see Fig. 7b).

If the moderators in the stack are separated by a gap d , as shown in (Fig. 25b), the mutual shadowing of the moderator surfaces is significantly reduced. When the gap d is approximately equal to the moderator width W , the mutual shadowing is reduced to a few percent (for the typical moderator size of about 10 cm). In this case, each moderator can be considered as practically fully illuminated by thermal neutrons. However, from the perspective of a neutron guide, this assembly of moderators appears as a moderator with a dead area (hole) of size d at the center. As a result, the average brightness of the moderator assembly is affected and is significantly reduced compared to the brightness of a single moderator:

$$B_{tot} = \frac{2I_1}{2W + d} < B_1 = \frac{I_1}{W} \quad (11)$$

Indeed, neither of moderator assemblies shown in Fig. 25 provide any brightness gain compared to the brightness of a single equally wide moderator. To achieve a higher neutron intensity while maintaining the brightness of a narrow moderator, it is crucial to ensure well-developed and practically fully illuminated surfaces of the individual moderators in the assembly, while avoiding any non-emitting areas or holes.

This can be achieved by filling the gap between adjacent moderators, which is shown in Fig. 25b, with an additional similar moderator, but shifted sideways by its length, thus creating a chessboard structure (Fig. 26a). One can also achieve the gap-free configuration by arranging moderators in a staircase structure (Fig. 26b). Such moderator assemblies has a large effective width W_A equal to the total width of the closely stacked single moderators (e.g. $3W$ as shown in Fig. 26). The losses in thermal neutron illumination resulting from mutual shadowing are rather small, less than 10%, and discussed in Appendix B.

By arranging N single moderators like steps in the staircase or chessboard assembly, the brightness of each individual moderator is effectively maintained, while the intensities from each moderator are added up.

In a typical situation of the single cold para-hydrogen moderator, there is a correlation between the brightness and size of moderators, with specific brightness levels associated with particular moderator sizes, and vice versa. However, when using an assembly of moderators, we decouple these values: it becomes principally feasible for assemblies of any size to achieve any desired brightness level, and conversely, any desired brightness level can be achieved using assemblies of any size.

Suppose the brightness of a narrow moderator, B_{narrow} , is k times higher than the brightness B_{vol} of a voluminous one. Then, a moderator assembly (i.e., cold neutron source) of N individual narrow moderators provides such increased cold neutron brightness $B_A = B_{narrow} = kB_{vol}$, while having the same size as the voluminous moderator $W_{vol} = W_A = NW$. Since intensity is the product of brightness and size (see Eq. (5)), the intensity I_A delivered by such a moderator assembly increases proportionally to N relative to intensity of individual narrow moderator: $I_A = NI_{narrow}$. Thus, compared to the

intensity of voluminous moderator $I_{vol} = B_{vol}W_A$, the intensity I_A increases by a factor of k as well:

$$I_A = NI_{narrow} = NB_{narrow}W = NkB_{vol}W_A/N = kI_{vol}. \quad (12)$$

Indeed, the intensity delivered by the moderator assembly is increased as much as its brightness with respect to voluminous moderator. Detailed calculations of the intensity delivered by a moderator assembly is presented in Sect. 6.3.

Alternatively, a staircase geometry (Fig. 26b) can be employed, where the lateral shift of all individual moderators (staircase steps) reduces their shadowing by neighboring moderators. This geometry may prove to be even more efficient, especially when used with thermal neutron moderators of large length.

The concept of using a moderator assembly with increased size and improved illumination addresses the need for enhancing the performance of low Q-resolution intensity-hungry instruments at a low-dimensional cold neutron source. This approach also effectively resolves the issue of under-illumination at the entrance of a large neutron guide. For example, in the case of the chessboard geometry shown in Fig. 26a, the effective cold neutron source width would be $3W$ — this ensures that the entrance of the neutron guide is sufficiently illuminated, enabling a better quality of the outgoing neutron beam.

It is important to note that for pulsed neutron sources, the staircase arrangement provides a notable increase in the effective neutron pulse length, because the propagation time of cold neutrons along a 15 cm long individual moderator is approximately 0.1–0.2 ms. While this may not have a significant impact on the pulse duration at long pulse neutron sources, it is problematic for short pulse neutron source³.

Certainly, narrow single high-brightness moderators can be assembled in various configurations depending on the specific requirements and design considerations. Fig. 27 illustrates some possible arrangements of these moderators, which can be used individually or combined in more sophisticated designs such as W - or V -arrangements for focusing or non-focusing purposes. These arrangements can be useful in the design of a high-brightness cold neutron source, particularly when aiming for a larger size and improved performance. As indicated in the reference [11], there exists a minimum cold neutron source size, denoted as D_{min} , for the optimal performance of each particular instrument. Through the use of assembly configurations, it becomes possible to employ several smaller moderators with enhanced brightness to meet this D_{min} requirement, resulting in an increased sample flux.

6.2. Brightness and intensity of moderator assembly

The intensity (total number of emitted neutrons) delivered by an individual moderator is calculated as the product of brightness and the moderator width. As depicted in Fig. 28a, a moderator with a width $W < 2$ cm provides a substantial 2–3 times increase in brightness compared to a voluminous moderator with dimensions of 10×10 cm² (black squares) by the price of the delivered intensity being reduced by a factor of approximately 3 due to the smaller size of the moderator (Fig. 28a, red circles).

However, for an assembly of moderators with a total width of W_A , this reduction is completely compensated by the number $N = W_A/W$ of moderators in an assembly. This is illustrated by Fig. 28b, where brightness and intensity gains are plotted as a function of the number of steps $N \in [1 - 10]$ in a $W_A = 10$ cm assembly. Here black squares and red circles correspond to individual moderator (as in Fig. 28a), while blue triangles depict the intensity

³The authors are grateful to J.Voigt (JCNS, Forschungszentrum Jülich) for bringing this point to their attention.

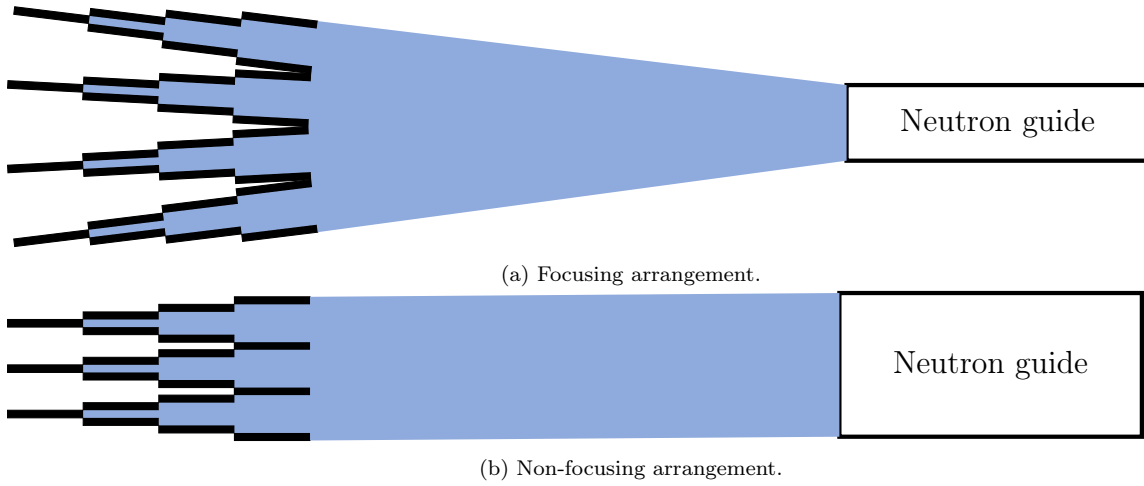


Figure 27: W-arrangements of single high-brightness moderators as a cold neutron source.

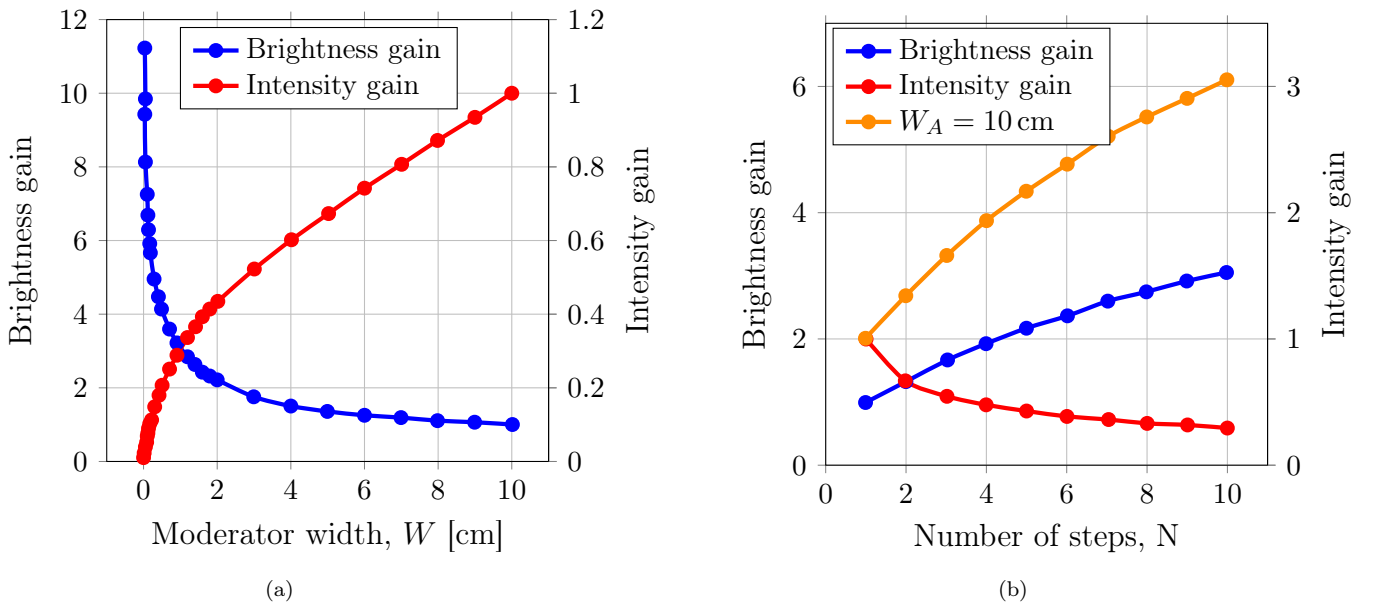


Figure 28: Brightness and intensity gains of individual moderators as a function of their width W (a) and number of steps N (b). Orange points represent intensity gains of a staircase or chessboard assembly with a width W_A of 10 cm. Solid lines are indicative.

gains of the N -step staircase assembly and all values are normalized to the respective values of the voluminous moderator with the same width $W_A = 10$ cm.

It is important to note, that brightness and intensity gains in Fig. 28b are equal, as it was already shown previously in Sect. 6.1 (see Eq. (12) and corresponding discussion). Indeed, the staircase and chessboard moderator assemblies provide a simultaneous, significant, and equal increase in both brightness and intensity, which is a distinct feature of this type of cold neutron source.

6.2.1. Procedure for brightness gain calculations

In the previous subsection, we presented the concept of chessboard and staircase moderator assemblies, each consisting of several individual moderators (steps). The overall brightness gain $G_{assembly}$ for such an assembly, compared to a voluminous moderator, can be calculated as the product of five independent factors:

$$G_{assembly} = G_{compression} \cdot G_{length} \cdot F_{position} \cdot F_{wall} \cdot F_{shadow}, \quad (13)$$

where $G_{compression}$ represents the compression gain of the moderator compared to a voluminous moderator with similar outer dimensions W_A and H , G_{length} is the length gain of the elongated para-hydrogen moderator, $F_{position}$ accounts for the non-uniformity in the incoming thermal neutron flux, F_{wall} accounts for wall losses and F_{shadow} accounts for the mutual shadowing of individual moderators. Below, we will discuss the first four factors, leaving the topic of shadowing for more detailed consideration in [Appendix B](#).

- Moderator compression.

Fig. 21 shows MCNP calculated brightness gains $G_{compression}$ depending on the moderator width. All results are normalized for $10 \times 10 \text{ cm}^2$ moderator. Results corresponding to moderator height 10 cm were fitted and that function was used for further calculations.

It's important to note, that due to identical outer dimensions of the entire moderator assembly, it can be placed in the same beam tube as a wide individual moderator, and does not require the modification of the position of surrounding reflectors. Indeed, the dependence of brightness gain on moderator sizes for individual moderators in assemblies is the same as for a voluminous moderator (see Fig. 21).

- Moderator length.

Para-hydrogen exhibits a very low scattering cross-section for cold neutrons. MFP for neutrons with $12 < E < 25 \text{ meV}$, where maximum of cold neutron spectrum is situated, can be estimated as $\lambda_{cold} = 10 \text{ cm}$ on average (Fig. 8). Indeed, the moderator brightness gain due to increased length can be estimated as

$$G_{length} = \int_0^L b(l) e^{-\lambda_{cold}/l} dl, \quad (14)$$

where $b(l)$ is the thermal neutron brightness in the position l .

- Thermal neutron flux distribution.

As mentioned earlier, the thermal neutron flux may vary along the moderator assembly. This variation imposes a limitation for the proposed moderator geometries, as the reduced thermal neutron illumination at the periphery of the staircase moderator assembly limits its feasible overall length and the number of individual moderators that can be used in the assembly (Fig. 29).

This limitation can be partially overcome by using multiple parallel staircase and chessboard assemblies, as shown in Figures 30c and 30d, respectively. In these figures, the overall assembly width W_A is kept constant, while the step width in multiple parallel staircases configuration is reduced. This leads to an increase in brightness from each step, although within limit defined by the wall thickness, as discussed below.

To incorporate the corresponding factor $F_{position}$ into calculations, the thermal flux distribution along the beam tube must first be defined. In the following sections, we will consider two types of distributions: one for heavy water reactor sources, with a typical full width at half maximum (FWHM) of 120 cm (Figures 29 and 33) and for spallation/compact neutron sources, with a typical FWHM of 25 cm (Fig. 37).

- Wall losses.

One of the factors decreasing the potentially achievable assembly brightness is the finite wall thickness of each individual moderator, which causes a reduction in the effective

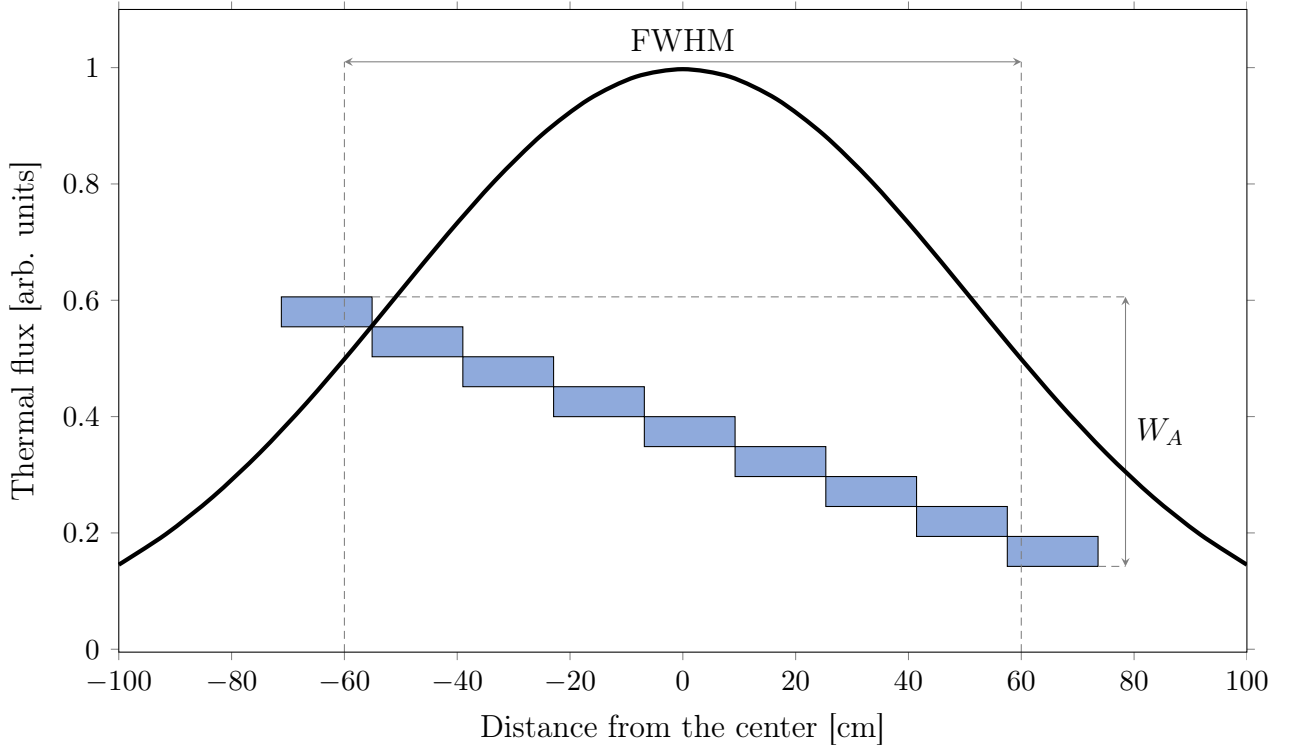


Figure 29: Thermal flux distribution for a typical thermal heavy water research reactor (shown in black) superimposed with the staircase moderator assembly layout.

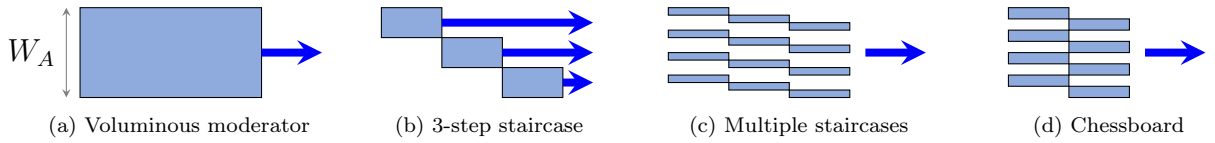


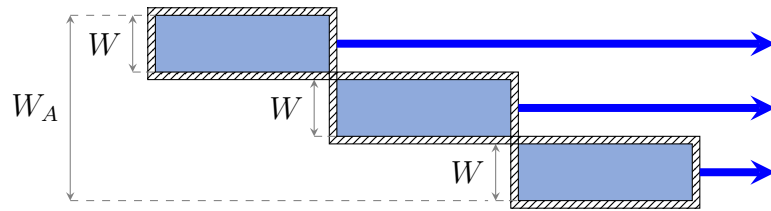
Figure 30: Layouts of various moderator assemblies of the same total width W_A . Blue arrows indicate outgoing cold neutron beam direction.

emitting area of the assembled cold neutron source. The losses can be minimised when the horizontal walls of neighbouring moderators overlap with each other, as depicted in Fig. 31a. Losses due to walls are proportional to the percentage of useful bright surface covered by walls:

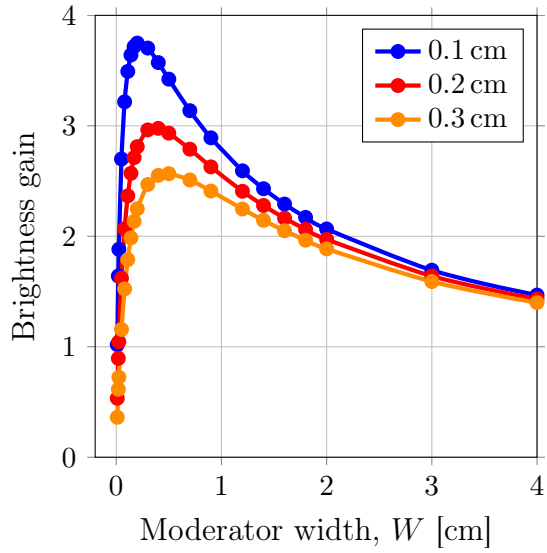
$$F_{wall} = 1 - a \frac{N - 1}{W_A}, \quad (15)$$

where F_{wall} is the remaining useful relative brightness, a is the wall thickness, N is the number of steps and W_A is the overall moderator width.

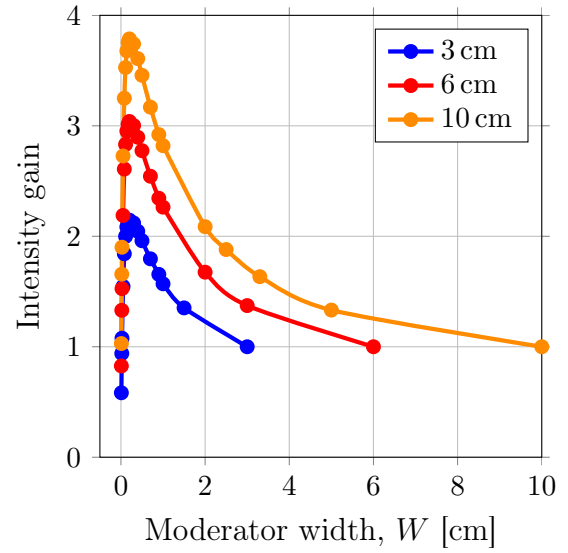
By multiplying this factor with the brightness gain dependence on the single moderator width W (as shown in Fig. 19), we can determine the reduced brightness gain for different wall thicknesses, which is presented in Fig. 31b for the moderator height $H = 10$ cm. While the brightness gain for a single moderator increases monotonically as its size decreases, considering the changes in wall thickness alters this dependence. For a given wall thickness, there exists a maximum achievable brightness gain, and this value increases as the walls become thinner. The step width should not be less than 0.25–0.5 cm (depending on wall thickness), limiting the allowable total number of steps in the assembly, e.g., to 12 for $W_A = 3$ cm and 40 for $W_A = 10$ cm (for a wall thickness of 1 mm).



(a) Overlap of horizontal walls of neighboring moderators.



(b) Brightness gain for various moderator wall thicknesses, normalised to the $10 \times 10 \text{ cm}^2$ moderator brightness (calculated based on the Fig. 21 data). Solid lines are indicative.



(c) Intensity gains achieved by moderator assemblies (with a wall thickness of 1 mm) compared to the intensity of voluminous moderators with the same width W_A (3, 6 and 10 cm). Solid lines are indicative.

Figure 31: Wall thickness effect.

Since the intensity gain of such assembly is calculated as the product of brightness and assembly width W_A , the finite wall thickness results in non-monotonic behavior of the intensity gain. It is illustrated in Fig. 31c, where intensity gains for different W_A are shown. One can see, that intensity gain for a 10 cm wide assembly consisting of 6 single 1.6 cm wide moderators is approximately 2.5 relative to the 10 cm wide voluminous moderator, and for a 6 cm wide assembly consisting of 4 single 1.5 cm wide moderators, the intensity gain is about 2 relative to the 6 cm wide voluminous moderator.

Consequently, using thinner walls proves to be advantageous. However, as parahydrogen in the moderator should be under high pressure, up to 20 bar [6], the thickness of the moderator walls should be sufficient for the safe operation of such moderators. Certainly, minimising the wall thickness poses a significant challenge and engineering efforts are needed to address it. One potential approach is to manufacture the single moderator from a single aluminium piece with internal ribs as shown in Fig. 32. These ribs serve the dual purpose of facilitating the proper flow of liquid hydrogen and acting as connectors between the large area surfaces of the moderator (approximately $10 \times 15 \text{ cm}^2$). This design enables the desired flow characteristics while potentially reducing the wall thickness to around 1 mm, thereby minimising the impact on brightness gain.

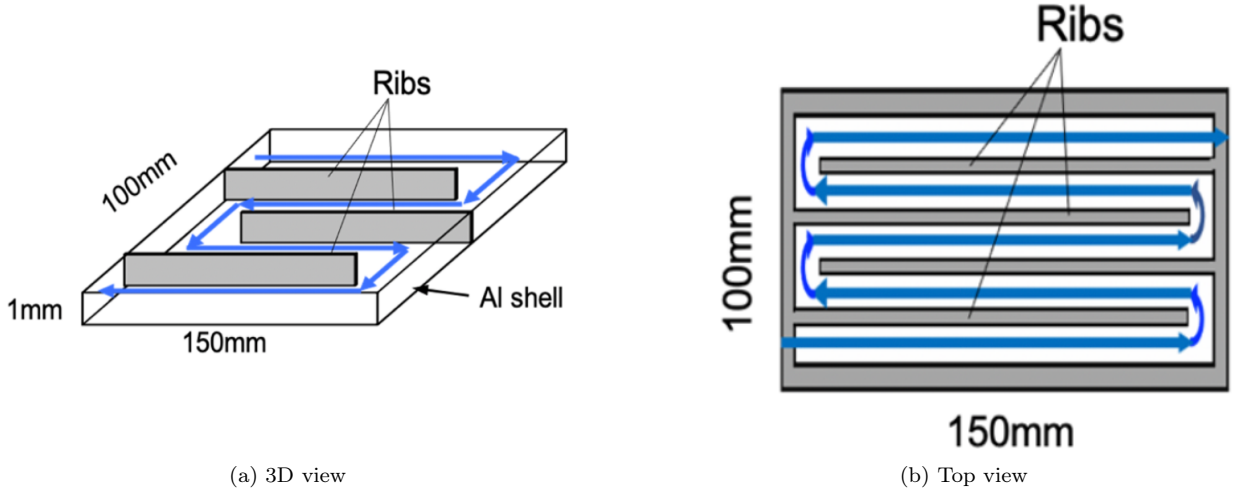


Figure 32: Conceptual drawing of thin narrow elongated cold moderator made of a single aluminum piece with vertical ribs connecting the thin upper and down large area surfaces. This design was suggested by Y. Bekler (Central Institute of Engineering, Electronics and Analytics (ZEA), Forschungszentrum Jülich).

6.3. Results

6.3.1. Moderator assemblies at reactor source

First, consider the brightness gains of single staircase moderator assemblies with different numbers of steps. These assemblies are installed in the beam tube of a heavy water research reactor with a thermal flux distribution of $\text{FWHM} = 120 \text{ cm}$ (as shown in Fig. 33). The results of calculations are presented in Fig. 34. All calculations are performed using Eq. (13), with the outer dimensions of the entire moderator assembly remaining constant.

The blue lines in Fig. 34 correspond to a 1 step moderator, essentially representing the behavior of a voluminous moderator (depicted as (a) in Fig. 33) with $H = 10 \text{ cm}$ and varying length. Its brightness increases with increased length until a certain point, after which it slowly decreases. This decrease is due to the following reason: since cold neutrons can only

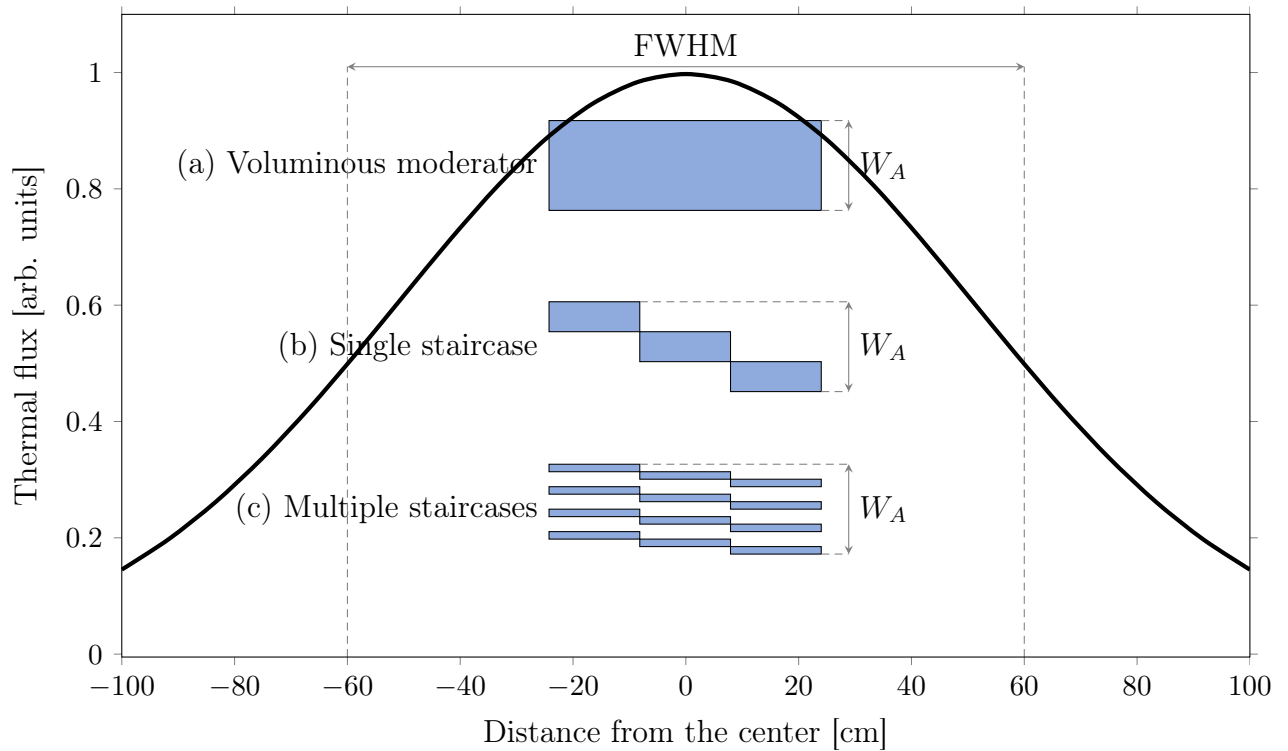


Figure 33: Typical thermal neutron flux distributions in a heavy water reactor (black curve), along with the placement of various moderator assemblies of equal overall width W_A .

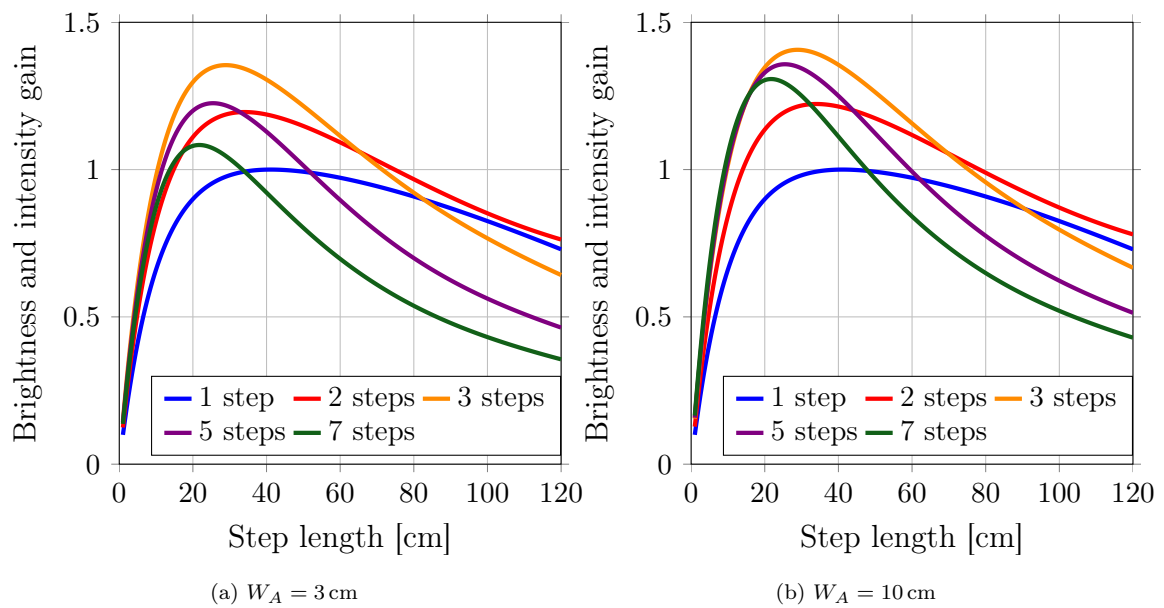


Figure 34: Overall brightness and intensity gain of various single staircase moderator assemblies with 1 mm wall thickness installed in a heavy water reactor as a function of step length.

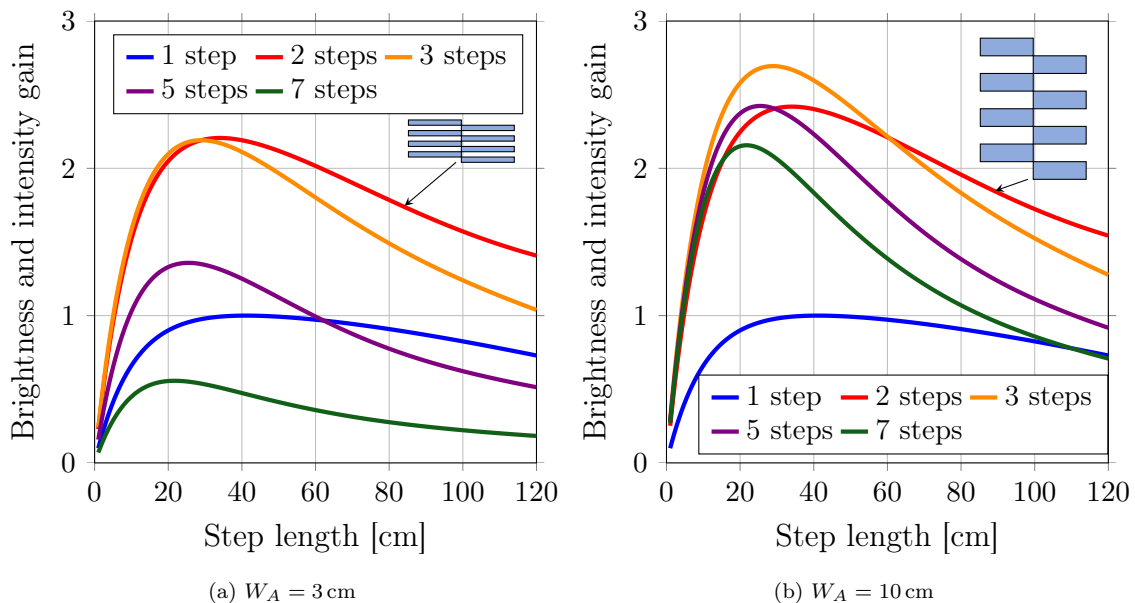


Figure 35: Overall brightness and intensity gain of various 4-staircase moderator assemblies with 1 mm wall thickness installed in a heavy water reactor as a function of step length.

be emitted from the moderator’s depth not exceeding 3 MFPs for cold neutrons, the emitting part of a long moderator is located outside the maximum thermal flux distribution region. The maximum of this 1 step function is taken as 1 and all other brightness functions shown in Fig. 34 are normalized by this value.

Fig. 34 also shows the overall brightness gains for single staircase moderator assemblies (depicted as (b) in Fig. 33) with a width W_A of 3 cm or 10 cm and a wall thickness of 1 mm. The calculated brightness of the assemblies is the average brightness over all steps. One can see that calculations are supporting the physical considerations in Sect. 6.1 and in general single staircase assemblies provide higher gains compared to the voluminous moderator. The 3-step configuration is most preferable, providing a relative gain of about 1.35 for 3 cm and 1.4 for 10 cm wide assemblies, so that their width doesn’t significantly influence the results. Brightness gains for smaller W_A are slightly lower because moderators’ walls occupy a larger relative part of the total assembly width.

Multiple parallel staircases assemblies provide higher gains than a single staircase arrangement. Fig. 35 shows potential gains for 4-staircase assemblies with an overall moderator width of $W_A = 3$ cm (a) and $W_A = 10$ cm (b). As before, the blue lines in these figures correspond to individual moderators of the same width and are used as a reference. As a visual aid, the two-step configurations corresponding to the red curves are depicted.

One can see that substantial additional gains can be achieved, e.g., $G_{assembly}$ up to 2.7 for $W_A = 10$ cm moderator assembly with 3 steps in each of 4 staircases (an additional factor of about 2 compared to a single staircase configuration). Such an assembly would consist of 12 individual moderators, each with a width of 0.8 cm, so that they provide high brightness.

For $W_A = 3$ cm, the gains are approximately 2.2 for both 2-step and 3-step staircases, each having different step lengths (note, that 2-step N -staircase configuration is essentially a chessboard configuration with $2N$ number of steps). The total length of the optimal assembly is about 70 cm. It’s noteworthy that, for the $W_A = 3$ cm moderator assembly with 5 steps on each of 4 stairs, the step width is only 0.15 cm. This corresponds to a significantly reduced brightness (see Fig. 31b and c) due to the wall effect, resulting in a substantial decrease in the brightness of such an assembly.

Notably, even relatively simple moderator assemblies composed of 4 individual moder-

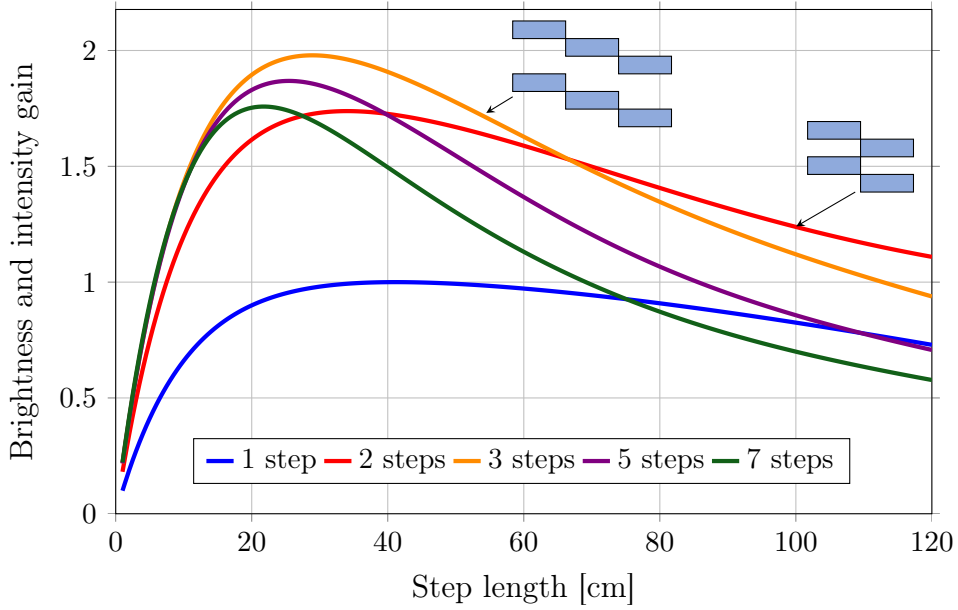


Figure 36: Overall brightness and intensity gain of various 2-staircase moderator assemblies with $W_A = 10$ cm and 1 mm wall thickness installed in a heavy water reactor as a function of step length.

ators in chessboard geometry yield significant enhancements in brightness and intensity of more than 70%, or gain of almost 1.7 (red curve in Fig. 36).

6.3.2. Moderator assemblies at spallation or compact sources

Now we examine a more compact thermal flux distribution, typical for spallation and compact neutron sources, and consider the performance of moderator assemblies illuminated by a thermal flux distribution with $\text{FWHM} = 25$ cm, as shown by the black curve in Fig. 37. As before, all calculations are performed using Eq. (13), with the outer dimensions of the entire moderator assembly remaining constant.

Fig. 38 shows brightness gains for single staircase moderator assemblies with an overall width of $W_A = 3$ cm and $W_A = 10$ cm, each with a wall thickness of 1 mm. Similar to plots in Fig. 34, the blue lines (1 step) represent the behavior of a voluminous moderator, which is depicted as (a) in Fig. 37. Note the sharp decrease in brightness (in contrast to the reactor case considered above) after a certain length. All brightness functions shown in Fig. 38 are normalised by the maximum value of the 1 step function for the corresponding assembly width. One can observe a notable reduction in achievable gains for single staircase configurations compared to the reactor case (Fig. 34), as there is limited space to shift individual moderators along the cold neutron beam axis. In this case a single staircase moderator assembly demonstrates no gain over conventional moderators.

A substantial enhancement in brightness can be achieved by employing moderator assemblies configured in chessboard or multiple parallel staircases geometry (see Fig. 30). In Figs. 40 and 39, brightness gains for chessboard and 4-staircase moderator assemblies (depicted in Fig. 37 as (c) and (d), respectively) with overall widths of $W_A = 3$ cm and $W_A = 10$ cm are presented. Similar to previous plots, these results are normalised by the maximum value of the 1 step function for the corresponding assembly width. One can see that for a simple V-shaped, 3-step chessboard moderator assembly, gains of about 1.4 are achievable. Note that since a V-shaped assembly consisting of three steps is not symmetrical with respect to the vertical axis, the gains for the V pointing in the outgoing beam direction (e.g. towards a neutron guide) are higher than in the opposite direction. This is because, in the first case, the end parts of the two moderators placed in the maximum

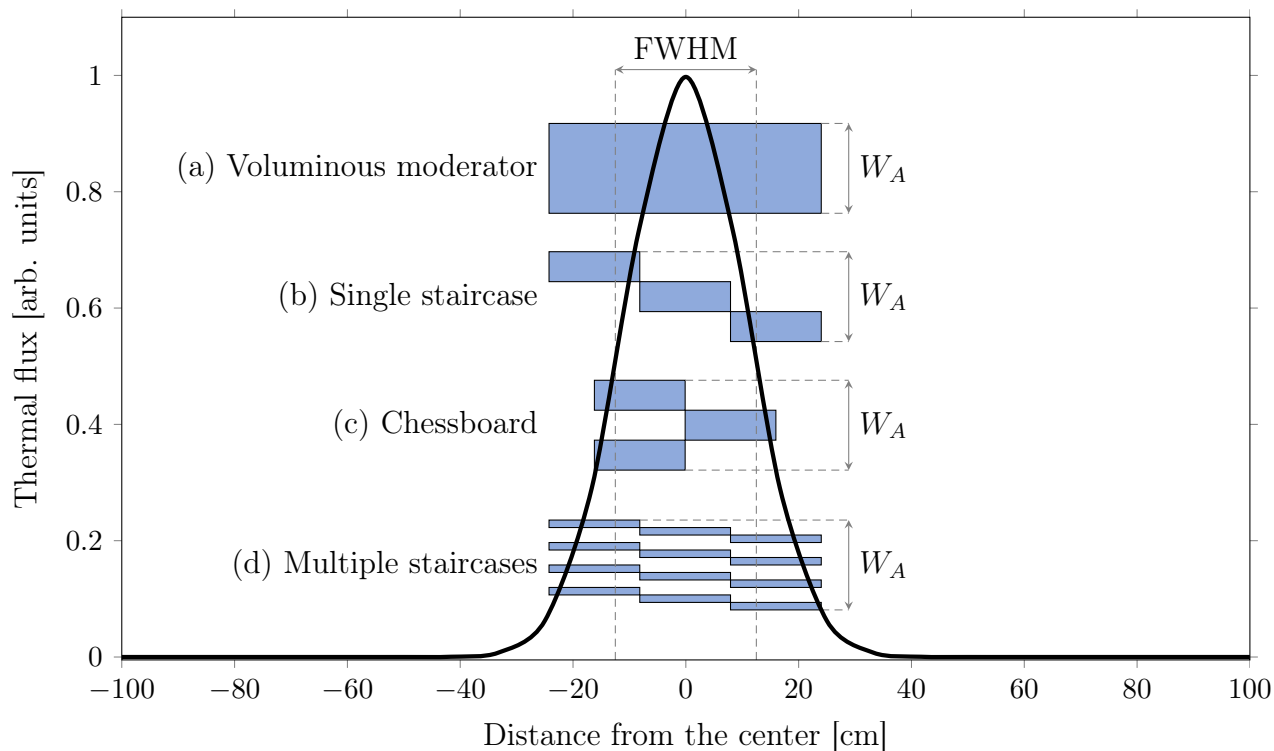


Figure 37: Typical thermal neutron flux distributions in spallation and compact neutron sources (black curve), along with the placement of various moderator assemblies of equal overall width W_A .

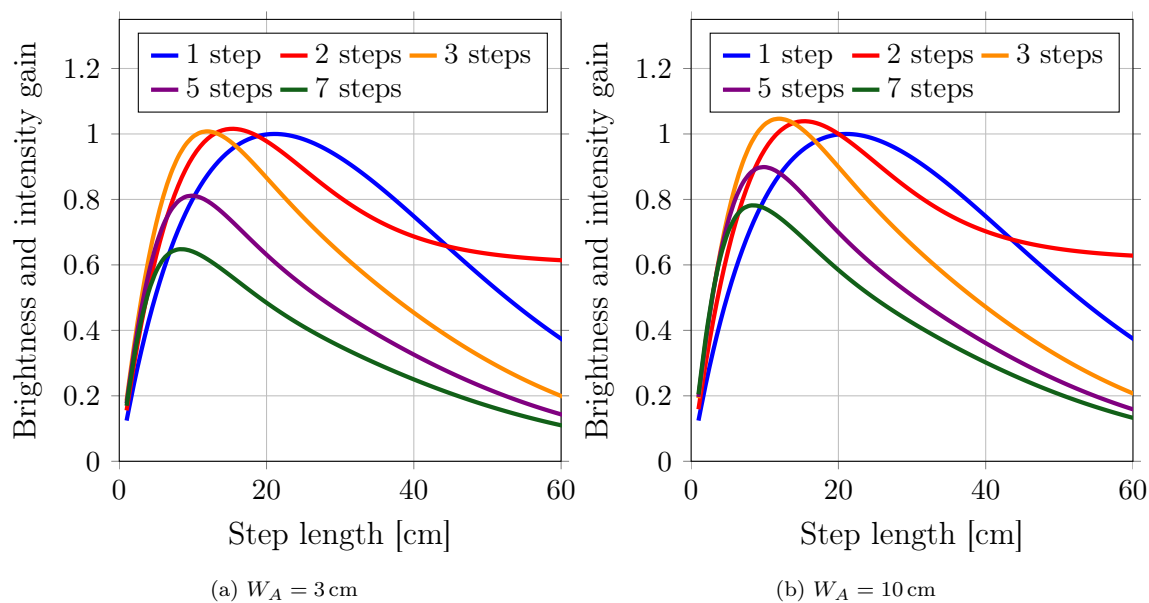


Figure 38: Overall brightness and intensity gain of various single staircase moderator assemblies with 1 mm wall thickness installed in a spallation or compact neutron source as a function of step length.

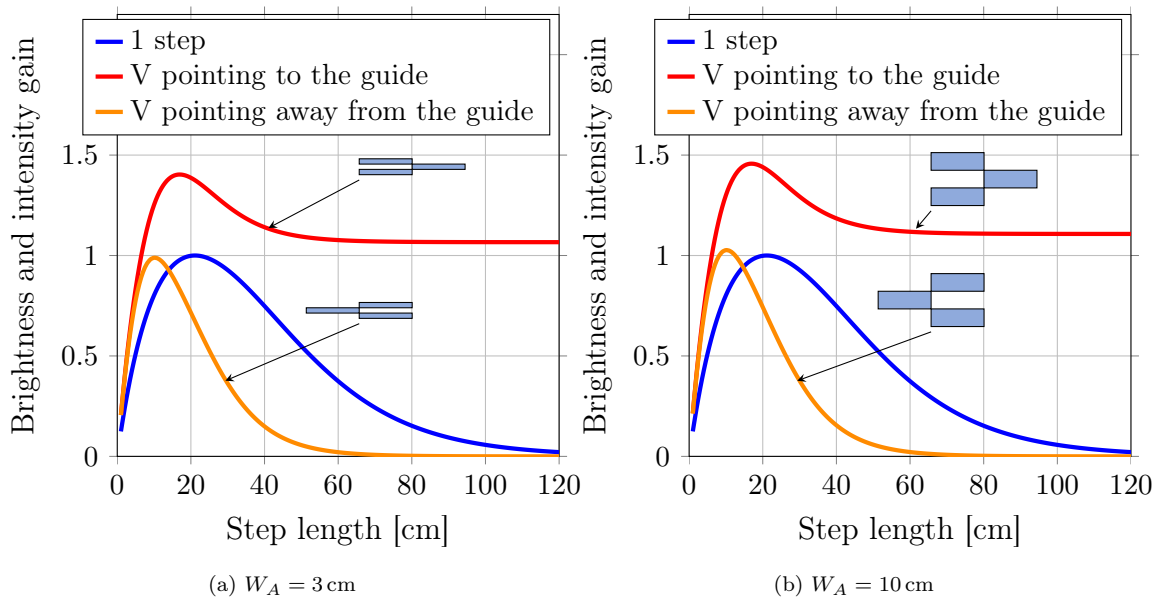


Figure 39: Overall brightness and intensity gain of chessboard moderator assemblies with 1 mm wall thickness installed in a spallation or compact neutron source as a function of step length.

thermal neutron flux distribution emit cold neutrons without further propagation through a thick layer of para-hydrogen, whereas in the second case, this occurs only for one moderator.

For the 4-staircase moderator assemblies (Fig. 40) gains about 1.9–2.1 are achievable. The staircases in optimal moderator assemblies would consist of 2 steps with step length $l_{step} \approx 18$ cm, each with a width of 0.37 cm for $W_A = 3$ cm and 1.2 cm for $W_A = 10$ cm, so that they provide high brightness (see Fig. 21). Note, that for $W_A = 3$ cm, 5-step staircases will have the step width of 0.15 cm, which corresponds to a significantly reduced brightness of individual moderators with the wall thickness of 0.1 cm and, consequently, in the absence of gain.

Note that the gains presented in this section may be further influenced by the specifics of the moderator-reflector assembly and should be evaluated through dedicated Monte Carlo simulations for a particular neutron source, which will be addressed in forthcoming publications.

Optimisation of the chessboard and staircase geometries for achieving their maximal performance should include determination of the optimal length and number of single moderators as well as specific gain values.

7. Conclusion and summary

Low-dimensional liquid para-hydrogen moderators, initially discovered and extensively developed at the ESS, enhance the brightness of cold neutrons compared to voluminous moderators [6]. Although this enhancement comes at the cost of reducing neutron beam intensity, it has been determined for the ESS instrumental suite [12] that the flat moderator with the smallest dimension of 3 cm, providing a brightness gain of about 2.5 with intensity losses of approximately 20%, offers a reasonable trade-off when considering various aspects of neutron beam extraction and transport to instruments. In this work, we focused on high-aspect ratio rectangular para-hydrogen moderators, where the width is much larger than its height (or vice versa). It was determined that due to the prevailing single-collision mechanism of the thermal-to-cold neutron conversion in para-hydrogen, the brightness gain for narrower moderators can reach rather high values, approximately around 10 (see Fig. 21).

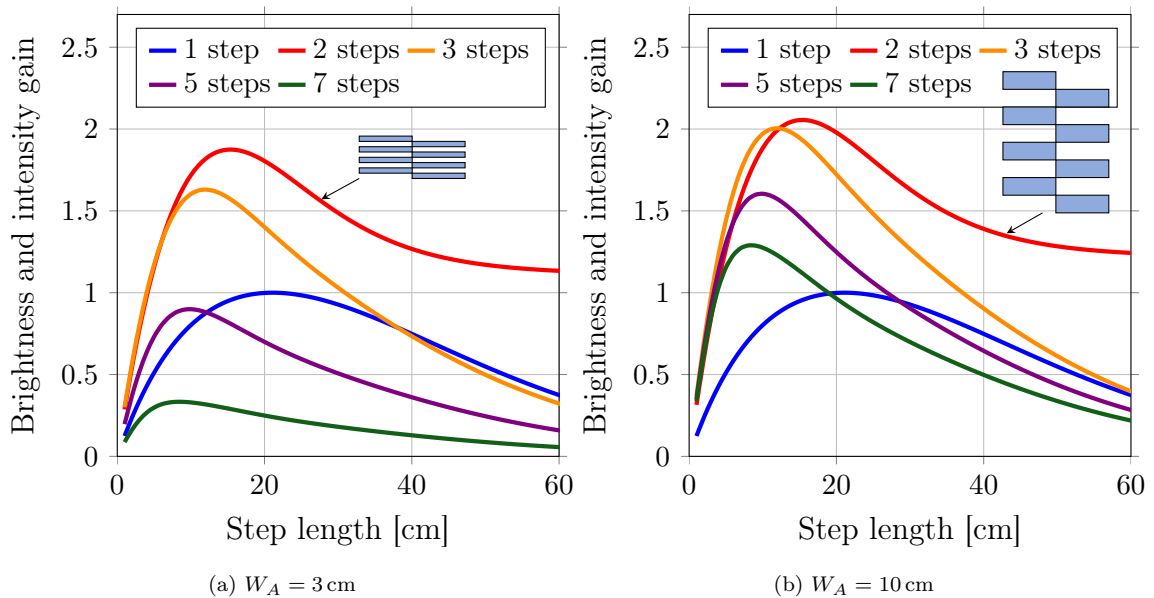


Figure 40: Overall brightness and intensity gain of 4-staircase moderator assemblies with 1 mm wall thickness installed in a spallation or compact neutron source as a function of step length.

However, these narrower moderators also exhibit even greater intensity losses and are not ideal from the perspective of neutron transport, mainly due to the insufficient illumination of the entries to neutron guides [11]. To address this challenge, we have introduced the concept of chessboard and staircase moderator assemblies with extensively developed total surfaces.

These assemblies generate wide neutron beams of higher intensity while preserving the enhanced brightness associated with high-aspect ratio individual moderators. Though a cold neutron source built upon such concept can principally provide an extremely high brightness, there is a practical limit of achievable brightness gain imposed by various factors including the moderator wall width and the limited volume of the high-density thermal neutron region surrounding the reactor core or spallation target. Analytic model calculations indicate that gains of up to approximately 2.5 in both brightness and intensity are achievable when compared to a source made of a single flat moderator with the same width. However, these gains will be affected by details of the moderator-reflector assembly and should be estimated through dedicated Monte Carlo simulations, which can only be conducted for a particular neutron source and are beyond the scope of this general study.

High brightness moderators assemblies can serve as not only primary components in new neutron sources but also as upgraded alternatives for the existing neutron guides in already established neutron sources. This approach allows for the optimization of neutron beam quality and intensity without needing to completely replace or rebuild existing neutron guide systems. The brightness dependency on moderator size is leading to the propagation of the “one instrument — one moderator” concept, where “brightness-hungry” instruments are placed on small moderators, while “flux-hungry” instruments are placed on larger ones. Implementing this approach in practice is quite demanding. The utilization of the suggested chessboard or staircase configurations partially addresses these challenges, introducing a novel “universal” moderator that is equally suitable for both brightness- and flux-hungry instruments. However, the relatively large length of moderator assemblies makes their application for short pulse neutron sources very problematic.

We have also explored the concept of “low dimensionality” in moderators, which yields a significant increase in brightness. We demonstrated that achieving this requires moderators to be low-dimensional both geometrically, implying a high aspect ratio, and physically, indi-

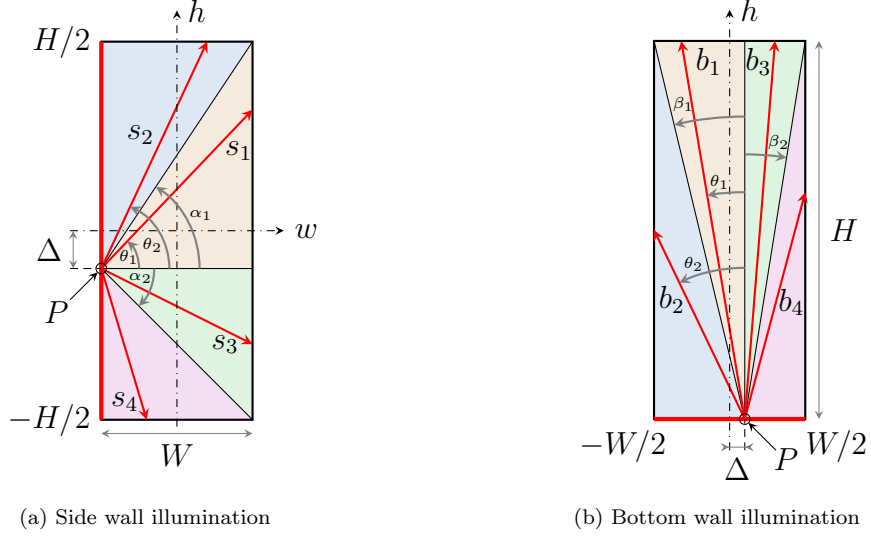


Figure A1: Notations used for calculating partial cold neutron intensities. Note that these diagrams do not depict angles θ_3 and θ_4 .

cating that the moderator's smallest dimension is smaller than the triple mean free path of thermal neutrons in para-hydrogen. This provides a physical explanation for the observed MCNP result: when the high aspect ratio moderator is additionally compressed along the longest direction, effectively giving it a tube-like shape, the resulting increase in brightness is only approximately 20 %.

Acknowledgement

This project was partially funded from the European Union's Horizon 2020 research and innovation programme under grant agreement No. 871072.

Appendix A. Total cold neutron intensity from rectangular moderator

Consider a moderator illuminated from the left side (Fig. A1a). The moderator area can be split into four segments, each shaded in different colours. The neutron path length s_i in each segment depends on the position of the thermal neutron emission point P , which is offset from the center of the emitting surface by a distance Δ . The inclination angles α_1 and α_2 of the lines connecting the neutron emission point P with the upper and lower corners of the moderator are defined as follows:

$$\alpha_1(\Delta, W, H) = \arctan\left(\frac{H/2 + \Delta}{W}\right) \quad (\text{A1})$$

$$\alpha_2(\Delta, W, H) = \arctan\left(\frac{H/2 - \Delta}{W}\right) \quad (\text{A2})$$

The neutron path lengths s_i in each segment are given as

$$s_1(\theta_1, W) = \frac{W}{\cos \theta_1} \quad (\text{A3})$$

$$s_2(\Delta, \theta_2, H) = \frac{H/2 + \Delta}{\sin \theta_2} \quad (\text{A4})$$

$$s_3(\theta_3, W) = \frac{W}{\cos \theta_3} \quad (\text{A5})$$

$$s_4(\Delta, \theta_2, H) = \frac{H/2 - \Delta}{\sin \theta_4} \quad (\text{A6})$$

where θ_{1-4} represent the angles between the normal to the emitting surface and the corresponding neutron paths, s_{1-4} . Assuming a constant thermal neutron flux distribution over the moderator surface, denoted as B_{th0} , the partial cold neutron intensities from these four segments are given as follows:

$$I_S^{(1)}(W, H) = B_{th0} \int_{-H/2}^{H/2} \int_0^{\alpha_1(\Delta, W, H)} \left(1 - \exp\left(-\frac{s_1(\theta_1, W)}{\Lambda_{th}}\right) \right) d\theta d\Delta \quad (\text{A7})$$

$$I_S^{(2)}(W, H) = B_{th0} \int_{-H/2}^{H/2} \int_{\alpha_1(\Delta, W, H)}^{\pi/2} \left(1 - \exp\left(-\frac{s_2(\Delta, \theta_2, H)}{\Lambda_{th}}\right) \right) d\theta d\Delta \quad (\text{A8})$$

$$I_S^{(3)}(W, H) = B_{th0} \int_{-H/2}^{H/2} \int_0^{\alpha_2(\Delta, W, H)} \left(1 - \exp\left(-\frac{s_3(\theta_3, W)}{\Lambda_{th}}\right) \right) d\theta d\Delta \quad (\text{A9})$$

$$I_S^{(4)}(W, H) = B_{th0} \int_{-H/2}^{H/2} \int_{\alpha_2(\Delta, W, H)}^{\pi/2} \left(1 - \exp\left(-\frac{s_4(\Delta, \theta_4, H)}{\Lambda_{th}}\right) \right) d\theta d\Delta \quad (\text{A10})$$

The total cold neutron intensity is equal to the sum of all partial intensities:

$$I_S(W, H) = I_S^{(1)}(W, H) + I_S^{(2)}(W, H) + I_S^{(3)}(W, H) + I_S^{(4)}(W, H) \quad (\text{A11})$$

Consider the case where the moderator is illuminated from the bottom (Fig. A1b). It is important to note that the only difference from the previously considered side illumination is the interchange of the roles of height H and width W . Therefore, by substituting W for H in equations (A1)–(A6), one can immediately derive expressions for the inclination angles α_1 and α_2 :

$$\beta_1(\Delta, W, H) = \arctan\left(\frac{W/2 + \Delta}{H}\right) \quad (\text{A12})$$

$$\beta_2(\Delta, W, H) = \arctan\left(\frac{W/2 - \Delta}{H}\right) \quad (\text{A13})$$

and for neutron path lengths b_i in each segment:

$$b_1(\theta_1, H) = \frac{H}{\cos \theta_1} \quad (\text{A14})$$

$$b_2(\Delta, \theta_2, W) = \frac{W/2 + \Delta}{\sin \theta_2} \quad (\text{A15})$$

$$b_3(\theta_3, H) = \frac{H}{\cos \theta_3} \quad (\text{A16})$$

$$b_4(\Delta, \theta_2, W) = \frac{W/2 - \Delta}{\sin \theta_4} \quad (\text{A17})$$

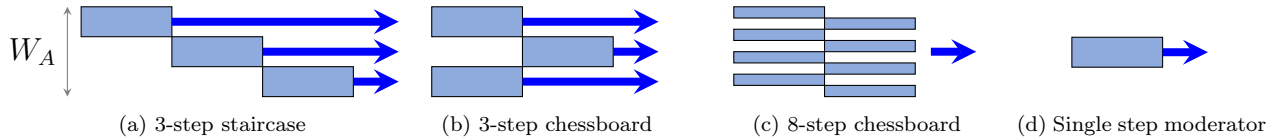


Figure B1: Layouts of moderator assemblies used to estimate the shadowing effect. Blue arrows indicate outgoing cold neutron beam direction.

where θ_{1-4} now represent the angles between the normal to the emitting surface and the corresponding neutron paths, s_{1-4} .

The partial cold neutron intensities from these four segments are given as follows:

$$I_B^{(1)}(W, H) = B_{th0} \int_{-W/2}^{W/2} \int_0^{\beta_1(\Delta, W, H)} \left(1 - \exp\left(-\frac{b_1(\theta_1, H)}{\Lambda_{th}}\right) \right) d\theta d\Delta \quad (\text{A18})$$

$$I_B^{(2)}(W, H) = B_{th0} \int_{-W/2}^{W/2} \int_{\beta_1(\Delta, W, H)}^{\pi/2} \left(1 - \exp\left(-\frac{b_2(\Delta, \theta_2, W)}{\Lambda_{th}}\right) \right) d\theta d\Delta \quad (\text{A19})$$

$$I_B^{(3)}(W, H) = B_{th0} \int_{-W/2}^{W/2} \int_0^{\beta_2(\Delta, W, H)} \left(1 - \exp\left(-\frac{b_3(\theta_3, H)}{\Lambda_{th}}\right) \right) d\theta d\Delta \quad (\text{A20})$$

$$I_B^{(4)}(W, H) = B_{th0} \int_{-W/2}^{W/2} \int_{\beta_2(\Delta, W, H)}^{\pi/2} \left(1 - \exp\left(-\frac{b_4(\Delta, \theta_4, W)}{\Lambda_{th}}\right) \right) d\theta d\Delta \quad (\text{A21})$$

The total cold neutron intensity for the bottom illumination is equal to the sum of these partial intensities:

$$I_B(W, H) = I_B^{(1)}(W, H) + I_B^{(2)}(W, H) + I_B^{(3)}(W, H) + I_B^{(4)}(W, H). \quad (\text{A22})$$

Appendix B. Shadowing effect

To estimate the shadowing effect of neighbouring steps, we compare the brightness of a single para-hydrogen step positioned alone in the centre of a long neutron beam extraction channel with that of the staircase or chessboard configuration (Fig. B1), where each individual step has a size of $(W_A/3 \times 10 \times 10)$ cm³.

The brightness spectra were calculated and utilised to determine integrated brightness values across various wavelength ranges (Table B1). Since the MFP for neutrons with wavelength 4–20 Å is larger than for neutrons with wavelength 3–4 Å (see Fig. 8b), the effect of shadowing for the former is smaller.

The shadowing factors are then calculated as the loss of brightness with respect to the single step moderator. Examples are shown in Fig. B2 and Table B2 for various wavelength ranges. As can be seen, the shadowing for cold neutrons with wavelengths in the range of 4–20 Å is less than 8% for both discussed moderator widths. Since we did not conduct the MCNP calculations for all possible staircase and chessboard configurations discussed in Sect. 6, we will assume a conservative estimate for the shadowing factor as $F_{shadow} = 10\%$ and use it for calculations. Note, that in the range of shorter wavelengths for the narrow, 3 cm moderator assembly, the shadowing is slightly higher, 15%.

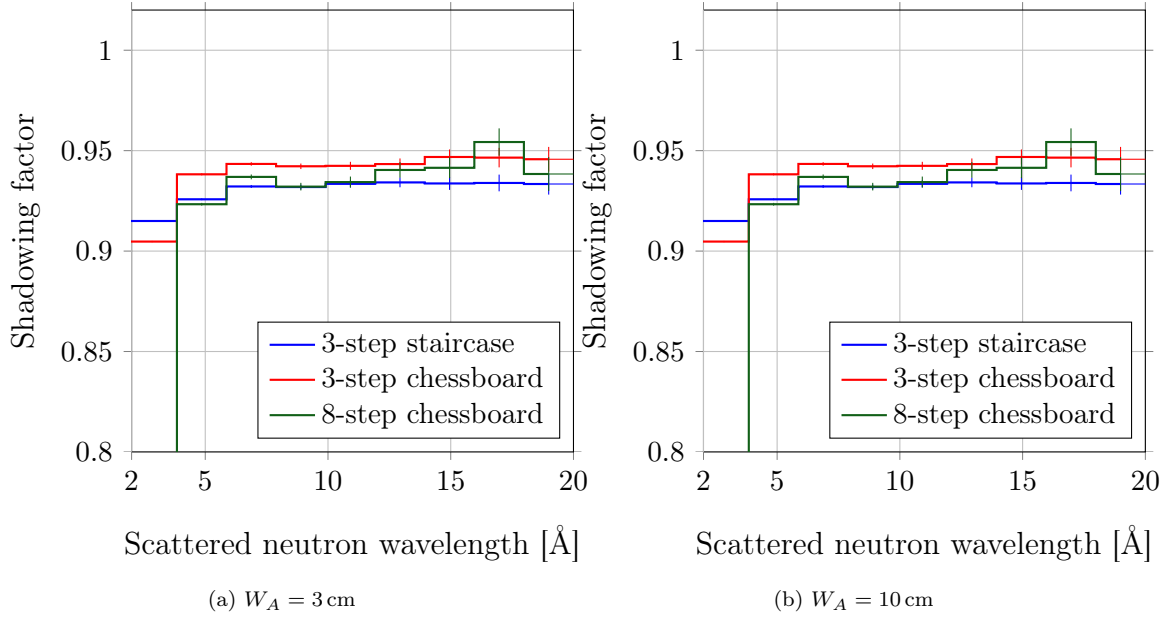


Figure B2: Shadowing factors as functions of neutron wavelength for selected configurations.

		$W_A = 3 \text{ cm}$		$W_A = 10 \text{ cm}$	
Layout	Figure	3–4 Å	4–20 Å	3–4 Å	4–20 Å
3-step staircase	B1a	1.452(3)	1.842(3)	1.242(2)	1.652(2)
3-step chessboard	B1b	1.462(3)	1.865(3)	1.247(2)	1.646(2)
8-step chessboard	B1c	1.349(3)	1.837(3)	1.212(2)	1.690(2)
Single step	B1d	1.578(3)	1.984(3)	1.302(2)	1.701(2)

Table B1: Central step brightness [$1/(\text{Å}^2 \text{ cm}^2 \text{ sr})$] for different moderator layouts.

		$W_A = 3 \text{ cm}$		$W_A = 10 \text{ cm}$	
Layout	Figure	3–4 Å	4–20 Å	3–4 Å	4–20 Å
3-step staircase	B1a	8.23(4) %	7.17(3) %	4.77(3) %	2.89(3) %
3-step chessboard	B1b	7.39(4) %	5.99(4) %	4.48(3) %	3.28(3) %
8-step chessboard	B1c	14.27(6) %	7.14(5) %	6.99(5) %	0.55(4) %

Table B2: Shadowing factors for staircase and chessboard arrangements.

References

- [1] Y. Kiyanagi, M. Ooi, H. Ogawa, M. Furusaka, Development of hydrogen cold moderator systems for a spallation neutron source, *Journal of Neutron Research* 11 (1–2) (2003) 3–11. doi:10.1080/1023816031000100860.
- [2] P. Ageron, P. De Beaucourt, H. Harig, A. Lacaze, M. Livolant, Experimental and theoretical study of cold neutron sources of liquid hydrogen and liquid deuterium, *Cryogenics* 9 (1) (1969) 42–50. doi:10.1016/0011-2275(69)90257-4.
- [3] Y. Shin, C. Lavelle, W. M. Snow, D. V. Baxter, X. Tong, H. Yan, M. Leuschner, Measurements of the neutron brightness from a phase II solid methane moderator at the LENS neutron source, *Nuclear Instruments and Methods in Physics Research Section A: Accelerators, Spectrometers, Detectors and Associated Equipment* 620 (2–3) (2010) 375–381. doi:10.1016/j.nima.2010.03.108.
- [4] K. Batkov, A. Takibayev, L. Zanini, F. Mezei, Unperturbed moderator brightness in pulsed neutron sources, *Nuclear Instruments and Methods in Physics Research Section A: Accelerators, Spectrometers, Detectors and Associated Equipment* 729 (2013) 500–505. doi:10.1016/j.nima.2013.07.031.
- [5] F. Mezei, L. Zanini, A. Takibayev, K. Batkov, E. Klinkby, E. Pitcher, T. Schönfeldt, Low dimensional neutron moderators for enhanced source brightness, *Journal of Neutron Research* 17 (2) (2014) 101–105. doi:10.3233/JNR-140013.
- [6] L. Zanini, K. Andersen, K. Batkov, F. Mezei, A. Takibayev, E. Klinkby, T. Schönfeldt, Design of the cold and thermal neutron moderators for the European Spallation Source, *Nuclear Instruments and Methods in Physics Research Section A: Accelerators, Spectrometers, Detectors and Associated Equipment* 925 (2019) 33–52. doi:10.1016/j.nima.2019.01.003.
- [7] K. Batkov, A. Takibayev, L. Zanini, F. Mezei, Cold moderators for long pulse neutron sources: unperturbed brightness, in: *International Topical Meeting on Nuclear Applications of Accelerators (AccApp–XI)*, Bruges, Belgium, 2013.
- [8] F. X. Gallmeier, I. Remec, A liquid hydrogen tube moderator arrangement for SNS second target station, *Review of Scientific Instruments* 93 (8) (2022). doi:10.1063/5.0095900.
- [9] U. Rucker, T. Cronert, J. Voigt, J. Dabruck, P.-E. Doege, J. Ulrich, R. Nabbi, Y. Beßler, M. Butzek, M. Büscher, et al., The Jülich high-brilliance neutron source project, *The European Physical Journal Plus* 131 (1) (2016) 19. doi:10.1140/epjp/i2016-16019-5.
- [10] E. Moskvina, N. Grigoryeva, N. Kovalenko, S. Grigoryev, Conceptual design of a time-of-flight powder diffractometer for a compact neutron source, *Journal of Surface Investigation: X-ray, Synchrotron and Neutron Techniques* 17 (4) (2023) 804–809. doi:10.1134/S1027451023040109.
- [11] P. Konik, A. Ioffe, A new method to find out the optimal neutron moderator size based on neutron scattering instrument parameters, *Nuclear Instruments and Methods in Physics Research Section A: Accelerators, Spectrometers, Detectors and Associated Equipment* 1056 (2023) 168643. doi:10.1016/j.nima.2023.168643.

- [12] K. H. Andersen, M. Bertelsen, L. Zanini, E. B. Klinkby, T. Schönfeldt, P. M. Bentley, J. Saroun, Optimization of moderators and beam extraction at the ESS, *Journal of applied crystallography* 51 (2) (2018) 264–281. doi:10.1107/S1600576718002406.
- [13] J. T. Goorley, et al., Initial MCNP6 Release Overview, *Nuclear Technology* (180) (2012) 298–315. doi:10.13182/NT11-135.
- [14] S. Mattauch, A. Ioffe, D. Lott, L. Bottyán, J. Daillant, M. Markó, A. Menelle, S. Sajti, T. Veres, HERITAGE: the concept of a giant flux neutron reflectometer for the exploration of 3-d structure of free-liquid and solid interfaces in thin films, *Nuclear Instruments and Methods in Physics Research Section A: Accelerators, Spectrometers, Detectors and Associated Equipment* 841 (2017) 34–46. doi:10.1016/j.nima.2016.09.043.
- [15] Y. Ikeda, J-PARC status update, *Nuclear Instruments and Methods in Physics Research Section A: Accelerators, Spectrometers, Detectors and Associated Equipment* 600 (1) (2009) 1–4. doi:10.1016/j.nima.2008.11.019.
- [16] N. Watanabe, Neutronics of pulsed spallation neutron sources, *Reports on Progress in Physics* 66 (3) (2003) 339. doi:10.1088/0034-4885/66/3/202.
- [17] J. L. Conlin, D. K. Parsons, F. B. Brown, R. E. MacFarlane, R. C. Little, M. C. White, Continuous $S(\alpha, \beta)$ Capability in MCNP, in: ANS Annual Meeting, Chicago, IL, USA, 2012.
- [18] M. Chadwick, P. Obložinský, M. Herman, N. Greene, R. McKnight, D. Smith, P. Young, R. MacFarlane, G. Hale, S. Frankle, A. Kahler, T. Kawano, R. Little, D. Madland, P. Moller, R. Mosteller, P. Page, P. Talou, H. Trellue, M. White, W. Wilson, R. Arcilla, C. Dunford, S. Mughabghab, B. Pritychenko, D. Rochman, A. Sonzogni, C. Lubitz, T. Trumbull, J. Weinman, D. Brown, D. Cullen, D. Heinrichs, D. McNabb, H. Derrien, M. Dunn, N. Larson, L. Leal, A. Carlson, R. Block, J. Briggs, E. Cheng, H. Huria, M. Zerkle, K. Kozier, A. Courcelle, V. Pronyaev, S. van der Marck, ENDF/B-VII.0: Next generation evaluated nuclear data library for nuclear science and technology, *Nuclear Data Sheets* 107 (12) (2006) 2931–3059. doi:10.1016/j.nds.2006.11.001.
- [19] H. Würz, Untersuchungen zur Neutronenthalisierung an flüssigem Ortho- und Para-Wasserstoff, 1973, KFK 1697, <https://d-nb.info/1187253243/34>.